Long-term variability of the coastal ocean stratification in the Gulf of Naples: Two decades of monitoring the marine ecosystem at the LTER-MC site, between land and open Mediterranean sea

Florian Kokoszka[1], Baptiste Le Roux[2], Daniele Iudicone[1], Fabio Conversano[1], and Maurizio Ribera d'Alcalá[1]

[1]Stazione Zoologica Anton Dohrn
[2]Ecole Centrale de Nantes

November 22, 2022

Abstract

We analyze 20 years (2001-2020) of temperature and salinity profiles at the LTER-MC coastal station in the Gulf of Naples, Mediterranean Sea. Surface and bottom layer show increases of temperature (+0.01 and +0.03°C/year, 2005-2019); water-columns budgets (heat, freshwater) show pseudo-periodic oscillations every 3 to 5 years, and weak linear trends. Seasonal minimum of salinity occurs two months later than the runoff peak, pointing to the importance of horizontal circulation in regulating the inshore-offshore exchanges and the residence time of freshwater contribution. Inter-annual variations of the mixed layer depth (MLD) exhibit a shallowing (-1.27m/year during winter) and a shortened time span of the fully mixed water-column. A visible decadal shift in the external forcings suggests an influence of winterly wind stress in 2010-2019, that prevailed over dominant buoyancy fluxes in 2001-2009. Changes are visible in the large-scale indices of the North Atlantic and Western Mediterranean Oscillations and highlight the role of wind direction, offshore or inshore oriented, in disrupting the stratification driven by freshwater runoff. A random forest regression confirms that role and quantifies the MLD drivers importances. This allows for a reliable prediction of the stratification using external variables independent from the in situ observations.

Long-term variability of the coastal ocean stratification in the Gulf of Naples: Two decades of monitoring the marine ecosystem at the LTER-MC site, between land and open Mediterranean sea

Florian Kokoszka[1], Baptiste Le Roux[2], Daniele Iudicone[1], Fabio Conversano[1], and Maurizio Ribera d'Alcalá[1]

[1]Stazione Zoologica Anton Dohrn, Naples, Italy
[2]Ecole Centrale de Nantes, Nantes, France

Acknowledgments

Data sets for this research are available presently on request, as the data paper is in preparation. We would like to thank the LTER-MC team that includes, besides the main authors: D. d'Alelio, C. Balestra, M. Cannavacciuolo, R. Casotti, I. Di Capua, F. Margiotta, M. G. Mazzocchi, M. Montresor, A. Passarelli, I. Percopo, M. Saggiomo, V. Saggiomo, D. Sarno, F. Tramontano, G. Zazo, A. Zingone, all based at Stazione Zoologica Anton Dohrn of Naples. Special thanks must be given to A. Passarelli and the commandants and crews of the R/V Vettoria for all their dedicated work at sea. The research program LTER-MC is supported by the Stazione Zoologica Anton Dohrn.

1 Abstract

We analyze 20 years (2001-2020) of temperature and salinity profiles at the LTER-MC coastal station in the Gulf of Naples, Mediterranean Sea. Surface and bottom layer show increases of temperature (+0 01 and +0.03 °C/year, 2005-2019); water-columns budgets (heat, freshwater) show pseudo-periodic oscillations every 3 to 5 years, and weak linear trends. Seasonal minimum of salinity occurs two months later than the runoff peak, pointing to the importance of horizontal circulation in regulating the inshore-offshore exchanges and the residence time of freshwater contribution. Inter-annual variations of the mixed layer depth (MLD) exhibit a shallowing (-1.27 m/year during winter) and a shortened time span of the fully mixed water-column. A visible decadal shift in the external forcings suggests an influence of winterly wind stress in 2010-2019, that prevailed over dominant buoyancy fluxes in 2001-2009. Changes are visible in the large-scale indices of the North Atlantic and Western Mediterranean Oscillations and highlight the role of wind direction, offshore or inshore oriented, in disrupting the stratification driven by freshwater runoff. A random forest regression confirms that role and quantifies the MLD drivers importances. This allows for a reliable prediction of the stratification using external variables independent from the in situ observations.

Keywords Ocean stratification, Time series, Mediterranean Sea, Coastal Ecosystem, Coastal observatory, Machine learning

Corresponding author: Florian Kokoszka, `florian.kokoszka@szn.it`

2 Introduction

Coastal areas represent $\sim$ 17% of marine primary production [Smith et al., 2005], contribute to the largest portion of fish catches ($\sim$ 80% if we consider all Large Marine Ecosystems as coastal systems, e.g., Sherman et al. [2009]), and provides for more than 90% of the global trade [WTO, 2018]. While the latter is sustained by the crucial role of maritime transportation, the former strongly depend on physical processes that occur in coastal systems. Winds, runoff, tides, heat fluxes (e.g., Ferrari & Wunsch [2009]) are the main source of auxiliary energy, sensu Margalef [1978] and Frontier et al. [2008], and modulate the large biogeochemical fluxes from land, through the atmosphere and runoff.

The presence and morphology of the land-ocean boundaries induce a high variability in abiotic and biotic components over spatial and temporal scales from daily to seasonal and inter-annual [Walsh, 1988]. Organisms must adapt to this range of time scales over which the availability of resources vary. At mid and at high-latitudes, a prominent driver of pelagic ecosystem is the seasonal cycle of the mixed layer [Sverdrup, 1953] even if the start of stratification is not the only trigger (e.g., Smetacek & Passow [1990], Behrenfeld [2010], Zingone et al. [2010]). Further to this cycle, coastal currents (e.g., Lentz [2012]), eddies (e.g., Kersalé et al. [2013]) and filaments (e.g., Iermano et al. [2012]) may modify the vertical structure of stratification, even without significant upwelling. Analyzing the processes regulating the water column structure in coastal ecosystems is therefore important, not only to assess the relative contributions of specific drivers in modulating the plankton dynamics depending on it, but also to attempt predicting how unique are the seasonal and regional characterization of the local dynamics (e.g., Sallée et al. [2021]).

Here, the challenge is to characterize the regional dynamical regime and to determine how it would be affected by changes in climate and anthropogenic activities. The Mediterranean sea is subject to warming and freshwater budget change (e.g., Bethoux et al. [1998]), and events such as the 2003 heatwave have been associated with strong stratification and inhibited mixing (e.g., Olita et al. [2007]). A general view indicates an increasing trend in the net heat content of the basin in the last decades (e.g., Criado-Aldeanueva et al. [2012]), with more frequent occurrences of heatwaves (e.g., Darmaraki et al. [2019]). This emphasizes the question on how the Mediterranean Sea responds in various climate change scenarios for the next decades, whether it will be dominated by a basin-scale response to the global atmospheric adjustments, or driven more regionally by local river runoffs and atmospheric forcings (e.g., Adloff et al. [2015]). In this context, an effort towards the development of climate indices and the improvement of long-term times series by in situ observations is of importance, for both open and coastal areas. Both heat and saline content are a primer (e.g., Iona et al. [2018]), but estimates of stratification from the water-column also have to be included to be compared to the observations in the upper 200 m during the recent decades (e.g., Guancheng et al. [2020]) and to separate the roles of thermal and saline contents. The Mediterranean Sea is an important zone for attempting projections [Giorgi & Lionello, 2007], as it has been identified as a major 'hotspots' for exhibiting the effects of climate changes Giorgi [2006].

There are many studies on the complexity of unique regional configurations for diverse marine coastal systems. For example, the recent work of Xiu et al. [2018] illustrates the case of the California Current System where wind and eddy activity in this specific area play a complex role in the redistribution and response of biological communities to nutrients supply. Each regional area is governed by specific physical and biogeochemical characteristics, establishing them as bioregions (e.g., El Hourany et al. [2021]) whose variability evolves with global warming. Systems in a Mediterranean climate are expected to become warmer and drier with climate change, where estuaries in these regions are predicted to experience variability in freshwater flows, such as 'marinisation' and hypersaline conditions (e.g., Hallett et al. [2018]). The Gulf of Naples (GoN) stands in this context. It is a coastal embayment opened to the Tyrrhenian Sea, with the Sarno river mouth on its South-West side, and the Volturno river flowing in the nearby Gulf of Gaeta. Importantly, the GON is the site of a monitoring point, 2 km off to the coast, sampled for more than thirty years as part of a LTER (Long-TERm) national network.

In our study, we look at the evolution of the water column structure over time to identify the physical processes whose sequence and interplay modulate the water column stability and drive the local variability. Our analysis exploits the last 20 years of a time series of physical parameters from a 70 m water-column, using weekly CTD profiles from 2001 to 2019. The stratification is described in terms of surface-bottom gradient and by the relative contribution of temperature and salinity, providing a different point of view than the common mean-state description. Disentangling the different contributions of temperature and salinity to the water buoyancy, we show the effect of climate on warming and freshening. The latter results, in a coastal environment such as the GoN, from changes in freshwater inputs, where modulations due to the ocean surface circulation are important. This allows us to establish the site as a good reference to project the impact of environmental forcing and anthropogenic activities on coastal systems and to differentiate the effects of each one. Specifically, here, we first describe the averaged seasonal climatological patterns, then the inter-annual variability, and focus in the third section on the seasonal drivers of the mixed layer in specific periods. To identify and assess the contribution of the relevant processes driving the mixed layer variability, external forcings such as wind stress and buoyancy fluxes are estimated over the area from the ERA5 data set. Finally, we propose to use external forcings as a set of predictors of the mixed layer through a random forest regression, to assess their relative weight and prepare for predictions in following studies.

3 Materials and Methods

3.1 Hydrological data set

Conductivity, temperature, and depth (CTD) profiles were carried out at the LTER-MC sampling point in the Gulf of Naples (**Fig. 1**) with a Seabird `SBE-911+` mounted on a 12-bottle carousel, with all sensors calibrated yearly. The raw 24 Hz profiles were processed using the standard Seabird software SeaSave to obtain bin-averaged data on a 1-m regular vertical grid. The weekly survey we use includes a total of 894 CTD profiles from the 4th January 2001 (cast MC465) to the 24th February 2020 (cast MC1359) (a calendar is available in supplementary Fig. S1). The Gibbs Sea Water (GSW) Oceanographic Toolbox (McDougall & Barker [2011]) was used to calculate the conservative temperature T_C (°C), the absolute salinity S_A ($\mathrm{g\,kg^{-1}}$), the water density ρ ($\mathrm{kg\,m^{-3}}$), the potential density σ_0 ($\mathrm{kg\,m^{-3}}$), the potential temperature θ_0 (°C), and the Brunt-Väisälä frequency N^2 ($\mathrm{s^{-2}}$). When mentioned thereafter, T and S refer to T_C and S_A. To provide a comparison in surface between the ocean coastal and open areas, we compare time series of temperature and salinity with the MedSea data reanalysis product extracted at the entrance of the Gulf of Naples (see the location in **Fig. 1**). The MedSea MFC physical reanalysis product (Escudier [2020]) is generated by a numerical system composed of an hydrodynamic model, supplied by the Nucleous for European Modelling of the Ocean (NEMO) and a variational data assimilation scheme (OceanVAR) for temperature and salinity with a horizontal grid resolution of 1/24° (i.e. 4-5 km) (`https://resources.marine.copernicus.eu/product-detail/MEDSEA_MULTIYEAR_PHY_006_004/INFORMATION`).

3.2 Water-column analysis: mixed layer depth, and budgets of heat, freshwater, and stratification contents

Mixed layer depth (MLD, meter) was calculated following the method of de Boyer Montégut et al. [2004] based on threshold values. Given a vertical profile of density $\sigma_0(z)$, or potential temperature $\theta_0(z)$, we calculated the depth below $z_{\mathrm{ref}} = 10$ m, where the profile reached thresholds defined as a cumulative of 0.4 °C for θ_0, and $0.03\,\mathrm{kg\,m^{-3}}$ for σ_0. A heat content HC ($\mathrm{J\,m^{-2}}$) and fresh water content FW (meter) are calculated for each CTD profile as $\mathrm{HC} = \int_{3m}^{65m} \rho(z)C_p(z)T(z)dz$ ($\mathrm{J\,m^{-2}}$), $\mathrm{FW} = \int_{3m}^{65m}(S^{+} - S(z))/S(z)dz$ (meter). Here $dz = 1\,\mathrm{m}$, $z_{\mathrm{bottom}} = 65\,\mathrm{m}$ and $z_{\mathrm{surface}} = 3\,\mathrm{m}$, the maximum and shallowest depth common to all profiles, $\rho(z)$ is the in situ density ($\mathrm{kg\,m^{-3}}$), $C_p(z)$ is the the specific heat capacity ($\mathrm{J\,kg^{-1}\,{}^{\circ}C^{-1}}$) calculated with the GSW functions (McDougall & Barker [2011]). Here the heat content estimate is not defined from a temperature change and cannot be interpreted as an absolute value. FW gives the amount of fresh water in meter to be added to the water-column to decrease the absolute salinity value from $S^{\max} = 38.65\,\mathrm{g\,kg^{-1}}$, a reference value above the maximum absolute salinity during the whole time series, to the observed depth-averaged salinity. To describe the stratification, a buoyancy anomaly content BC is calculated as the integral over depth of the density difference between each depth and the bottom: $\mathrm{BC} = \int_{3m}^{65m} \rho(z) - \rho_{\mathrm{bottom}} dz$ ($\mathrm{kg\,m^{-2}}$). The relative contributions of T and S to the buoyancy content is quantified as $\mathrm{BC} = \mathrm{BC}_T + \mathrm{BC}_S$, with $\mathrm{BC}_T = \int_{3m}^{65m} -\rho_* \alpha(T(z) - T_{\mathrm{bottom}})dz$, and $\mathrm{BC}_S = \int_{3m}^{65m} \rho_* \beta(S(z) - S_{\mathrm{bottom}})dz$, where $\rho_* = 1000\,\mathrm{kg\,m^{-3}}$, $\alpha(z)$ and $\beta(z)$ are the thermal expansion and saline contraction coefficients calculated with the GSW functions. Bottom values are values at the end of each profiles. We provide another complementary index to the buoyancy anomaly content, the stratification intensity IS, defined as the difference between surface and bottom for each CTD profile : $\mathrm{IS} = \sigma_{\mathrm{bottom}} - \sigma_{\mathrm{surface}}$.

3.3 Bulk parameters of the atmospherical forcings of the area : heat fluxes, precipitations, winds, and climatic indices

The net surface fluxes (Q_{net}, the total of latent and sensible heat, plus net solar and thermal radiation, in $\mathrm{W\,m^{-2}}$), wind velocities (U_{10} and V_{10}, $\mathrm{m\,s^{-1}}$), rates of evaporation E and precipitation P ($\mathrm{mm\,d^{-1}}$), period and significant height H_S of waves, were extracted from the ERA5 re-analysed product provided by Copernicus (ERA5(C3S) [2017]). The extraction is done at the closet grid-point from the LTER-MC geographical position ($14.25°E$ and $40.80°N$), with a 6-hour temporal resolution, from the 1st January 2001 and covering the whole period. A seasonal cycle of the surface heat content from fluxes (HF) is calculated by integrating Q_{net} in function of time: HF $= \int Q_{net}dt$.

The buoyancy flux B ($\mathrm{m^2\,s^{-3}}$, defined > 0 when B is stabilizing the water-column), is proportional to the density flux at the surface: $B = gQ_p/\rho_0$, where the density flux Q_p into the ocean from the atmosphere was computed as $Q_p = \rho(\alpha F_T + \beta F_S)$, with α and β the thermal expansion and saline contraction coefficients, respectively [H.-M. Zhang & Talley, 1998]. Here $F_T = -Q_{net}/\rho_{sea}C_p$, and $F_S = (E - P)S/(1 - S/1000)$, where C_p is the specific heat of seawater, E, P, and S are the evaporation, precipitation and sea surface salinity. The velocity friction u_* was calculated as $u_* = \sqrt{\tau/\rho_{sea}}$, where ρ_{sea} is the density of sea water, and τ the wind stress, as $\tau = \rho_{air}C_D U_{10}^2$, where $\rho_{air} = 1.22\ \mathrm{kg\,m^{-3}}$, and the drag coefficient C_D and the velocity at 10 m U_{10} are calculated from the wind speed following Large & Pond [1981].

The North Atlantic Oscillation (NAO) is responsible for changes in the geographical distribution of surface westerlies across the North Atlantic basin toward Europe (Hurrell [1995]), and we use the classical NAO index developed by Hurrell & Deser [2009] to describe these variations. Data were provided by the NOAA National Weather Service (`https://www.cpc.ncep.noaa.gov/products/precip/CWlink/pna/nao.shtml`). To link the Mediterranean basin dynamic to the Atlantic variability, we complete it with the Western Mediterranean Oscillation (WEMO), a pattern of atmospheric circulation described by Martin-Vide [2006], whose index corresponds to the difference in surface pressure between San Fernando (Spain) and Padua (Italy). Its variations can lead to a regime of winds blowing from the east (Bonifacio et al. [2019], e.g. case of the central European anticyclone located north of Italy, with a low-pressure center in the Iberian peninsula). Data were collected from `http://www.ub.edu/gc/English/wemo.htm.`

3.4 Temporal averaging and statistical fits

Property averages are calculated for different periods, defined here. The LTER-MC observations are made weekly : the day of the week for sampling depended on the sea and weather conditions, and was not necessarily the same (for example, MC465 was on Thursday 4th of January 2001, MC466 on Wednesday 10th, and MC467 on Tuesday 16th). To have the consistency of a regular temporal grid, we consider the week of the year number as a regular timestamp (1 to 52). The monthly average is defined as the mean of the parameter values for each month of the year over the years, from January to December (12 bins). Inter-annual average is the mean of the parameter values for each year, from 2001 to 2019 (19 bins). Average by seasons is the mean of parameters for the four monthly periods (March-May for spring, June-August for summer, September-November for autumn, and December to February of the following year for winter). For each bin, the standard error e_{std} can be calculated as the standard deviation σ_{std} of the N_{b} values as $e_{\mathrm{std}} = \sigma_{\mathrm{std}}/\sqrt{N_{\mathrm{b}}}$. Linear regressions and their associated statistics (slope, 95% confidence interval, p-value, correlation coefficient, R^2) were performed using the `linregress` functions from the Python library `scipy.stats` (Virtanen et al. [2020]). Identification of clusters was done with the `sklearn.cluster` function from the `KMeans` library (Pedregosa et al. [2011] ; `https://scikit-learn.org/stable/modules/clustering.html`). Ruptures in time series are investigated using the Python library `ruptures` for off-line change point detection (Truong et al. [2020]; `https://pypi.org/project/ruptures/`), and T-Test are calculated with the `t` functions from `scipy.stats`.

3.5 Machine Learning : a random forest regression

To assess the weight of various independent contributors to the MLD dynamics, and identify which processes dominate, we perform a random forest regression (Pedregosa et al. [2011]). This ensemble method fits a number of decision trees on various sub-samples of the data set and allows to obtain a score to input features and their importance based on how useful they are to predict a chosen variable. To modelize the MLD at the site we select input variables that are nearly-independent from the in situ observations to be able to apply the forecasting tool to projections. To correlate consistently the observations to the forcings, the latter are averaged on the interval period between each MC cast (for example, forcings at MC466 are the average between MC465 and MC466, i.e. between the 5th (4th+1) and 10th of January). We use seven parameters (week of the year, wind direction, wind stress, buoyancy fluxes, sea surface temperature, sea surface salinity outside the gulf, and net precipitation rates) estimated with the bulk parameters from ERA5. Their importance in the fitting is then determined as the Gini importance in %, Breiman [2001]. We perform various training by splitting the time series in decades (2001-2009 as decade I, and 2010-2019 as decade II), and seasons (months of March-May for spring, June-August for summer, September-November for autumn, and December to February of the following year for winter). Training is realized on 80% of the data available by subset, the 20% remaining being used for the validation. Each training parameter is normalized to range its minimum and maximum from 0 to 1 (or -1 to 1 for signed quantities). Performance of the training is determined by comparing the MLD estimates to the monthly climatological values (i.e. the monthly atlas we could refer to, in case we would not have in situ observations). Calculations are achieved through the `RandomForestRegressor` function from the `sklearn.ensemble` module (`https://scikit-learn.org/stable/modules/generated/sklearn.ensemble.RandomForestRegressor.html`). Statistics of the training are given in the **Tab. 3**).

4 Results

4.1 Ocean climatology of the LTER-MC station

4.1.1 Coastal vs. open area : difference in the surface salinity between the Gulf of Naples and the open Tyrrhenian Sea

To introduce the time series analyses we carry on, we start with characterizing the coastal and offshore water properties by comparing the difference between the seasonal cycle of surface temperature and salinity obtained from the observations in the GoN from 2001 to 2019, and the MedSea data reanalysis product, extracted in the Tyrrhenian Sea during the same period (see the two locations in **Fig. 1**). Seasonality of the sea surface temperature is comparable (**Fig. 2, top left**), though with around 1 °C difference in summer, but shows a difference in the cycle of surface salinity, not only in amplitude, but also the phase (**Fig. 2, top right**). As it can be expected, from April to November coastal waters are fresher than the offshore from around $0.15\,\mathrm{g\,kg^{-1}}$ to $0.35\,\mathrm{g\,kg^{-1}}$, but surface minimum and maximum occur in May-June and in September (respectively), with a delay of around one month compared to the Tyrrhenian area. This simple plot emphasizes the importance of fresh runoffs to the salinity cycle as observed at the LTER-MC point in the GoN, and the probable presence of horizontal advection mechanisms that partially mitigate the offshore to inshore gradient and limit the exchanges of salt.

4.1.2 Seasonal hydrology in the GoN

Seasonal variations of salinity show a minimum of $37.4\,\mathrm{g\,kg^{-1}}$ occurring into the first 10 m of the surface layer from May to June (**Fig. 2, bottom**). Maximum value of $38.2\,\mathrm{g\,kg^{-1}}$ is in January. A remarkable salty layer with values close to the maximum, between 38.1 and $38.2\,\mathrm{g\,kg^{-1}}$ is visible from September to November, below 10 m depth and above the 20 m to 50 m layer of relative less salty water ($38.0\,\mathrm{g\,kg^{-1}}$). The thickness of this salty tongue increases in time following the deepening of the seasonal thermocline up to November, progressively filling the water column, besides the first 5 m which display a less salty water of 37.4 to $37.8\,\mathrm{g\,kg^{-1}}$. Intrusions of salty water from 10 to 60 m create the conditions for salt-fingering below the MLD, as discussed by Kokoszka et al. [2021]. Temperature shows a more classical seasonal cycle. A maximum of 26.4 °C occurs in august (**Fig. 2, bottom**). High values decrease from 26.0 °C in July to 24.6 °C in September. Potentially unstable water parcels appear during winter at surface, from November to February, with the presence on the first 10 m of relatively cold water, of around 0.05 °C to 0.25 °C colder than the rest of the water column. Stabilization of the water column starts in March, after the annual minimum of 14.0 °C opening the spring-summer periods that exhibits a classical thermocline deepening to 20 m during the season. Black contours in **Fig. 2 (bottom)** shows the density estimates over the seasonal cycle. From January to April, density variation contours follow better the $\mathrm{MLD}_{\sigma_0}^{0.03}$ estimation (**Fig. 2, bottom, plain white lines**), where the superscript defines the chosen σ_0 threshold value to determine MLD (see Methods). From May to September, MLD estimate falls within the 10m-depth limit, in good agreement with density field. From October to December, the visual fit would lead to a steeper variation than the two criteria above. When relying on the temperature-based estimate (**Fig. 2, bottom, dashed white lines**), effect of salty layers is not taken properly into account and seasonal cycle estimation follows a sharper behaviour than the density-based one.

4.1.3 Seasonal budgets and environmental context of the GoN

The mean seasonal cycle of HC has a minimum in March, $1.05 \times 10^{8}\,\mathrm{J\,m^{-2}}$, and a maximum in October at $1.35 \times 10^{8}\,\mathrm{J\,m^{-2}}$ (**Fig. 3.a,b**). This cycle of the heat content is comparable to the ERA5 surface heat content from fluxes, once integrated in time. **Fig. 3.e** shows both HC and integrated HF cycles (centered on zero with the mean value being removed). Timing fit is different with the maximum of HC occurring in October, one month later than HF. Even if the net solar radiation dominates the fluxes, delay with the in situ estimation suggests clearly other contributors to the budget of the water-column. In terms of freshwater content, to reach the minimum of salinity in June, which is also the maximum deviation from a chosen reference value of $38.65\,\mathrm{g\,kg^{-1}}$ (**Fig. 3.b**), a FW addition of nearly 112 cm would be needed, and these values are 85 cm and 80 cm for December and January, respectively. The freshest value appears to be later than the maximum of atmospheric freshwater and river discharge, which occurs from February to April [Mariotti et al., 2002], and illustrated by the seasonal cycle of precipitation at the LTER-MC station (**Fig. 3.f**). Such delay is mostly due to the progressive accumulation of fresh water during the spring stratified period, which accumulates FW and concentrates it in a shallower water column. However, circulation may also contribute to occasionally decrease salinity by the horizontal advection of freshwater across the shelf via filaments, as showed by Iermano et al. [2012].

An indication of the whole column stability is given by IS the intensity of the stratification, whose seasonal cycle in **Fig. 3.c** presents a distribution centered on July-August. The minimum value is $0.06\,\mathrm{kg\,m^{-3}}$ in January, and the maximum of 3.32 and $3.38\,\mathrm{kg\,m^{-3}}$ is in July and August. Finally, we complete IS with the depth integrated buoyancy anomaly to the bottom (BC) that takes in account the full water-column content. In **Fig. 3.d**, BC presents a different distribution compared to IS, by being centered on September-October, to become steeper in December. This descriptor allows to discern between changes driven by buoyancy fluxes and involving the whole water column from processes occurring in different layers for internal mixing and lateral advection. This shows the difference between IS and BC from May to November, questioning about the choice of the best macro-index to use to describe the state of the stratification [Sallée et al., 2021]. In **Fig. 3.d**, BC is decomposed between temperature (red line) and salinity (blue line) to determine their relative weight. BC is mostly driven by the temperature gradient, which contributes to maximum difference of $64.2\,\mathrm{kg\,m^{-2}}$ in September, while salinity reaches its maximum contribution in June-July around $8.17\,\mathrm{kg\,m^{-2}}$, representing a factor of nearly 8 in favor to the temperature. But during the winter periods this dominant situation can invert and make salinity increasing its contribution by a factor 2 with respect to temperature. The main consequence of the salt contribution to the density is a limitation of the MLD estimates based on the density threshold, as showed on the mean salinity profiles in **Fig. 2 (bottom)**, where $\mathrm{MLD}^{0.03}_{\sigma_0}$ is generally shallower than $\mathrm{MLD}^{0.4}_{\theta_0}$ with the presence of relatively salty deeper layer. This situation refers to the commonly known case of barrier layer (Kara et al. [2000]), noticeably frequent in tropical areas (Vissa et al. [2013]), where MLD is overestimated when using temperature only, due to the seasonal contribution of salt to the density. Here this effect is due to dispersal of the runoff and not to direct precipitations, as in the open ocean.

We complete the description of the environmental context of the GoN with the seasonal cycles of the physical parameters associated to the atmospherical forcings in the **Fig. 4**. Total surface fluxes varies from $-100\,\mathrm{W\,m^{-2}}$ to $100\,\mathrm{W\,m^{-2}}$ with a maximum in June and a minimum and December-January, while shortwave fluxes, are maximal in June and July. Buoyancy fluxes reproduce this seasonal distribution and ranges in average from $-0.25{\times}10^{-7}\,\mathrm{W\,kg^{-1}}$ to $1{\times}10^{-7}\,\mathrm{W\,kg^{-1}}$, with a more regular increase from January to June and a steeper decrease from July to September. Sea waves and wind stress remarkably co-vary seasonally, the more intense seasons being winter (mean values of height of waves of 0.7 m and wind stress above $5{\times}10^{-3}\,\mathrm{m\,s^{-1}}$), while the quieter period is summer (mean values of height of waves of 0.4 m and wind stress close to $3{\times}10^{-3}\,\mathrm{m\,s^{-1}}$). Wind components have some interesting seasonal cycle, $\overline{u}$ being westward in winter (close and above $0.5\,\mathrm{m\,s^{-1}}$ from October to February), and eastward in summer (above $1\,\mathrm{m\,s^{-1}}$ from June to August). The component $\overline{v}$ has a different distribution, close to zero from February to June, southward in summer (close to $0.25\,\mathrm{m\,s^{-1}}$ from July to September) and winter (close to $0.5\,\mathrm{m\,s^{-1}}$ in December and January), and northward in November with speed close to $0.5\,\mathrm{m\,s^{-1}}$. This results in winds oriented toward East from May to August (angles close to 0° or 360°), toward West from December to February (close to 200°), and oriented toward the North quarter in March-April (180° to 0°), and turning toward the South quarter in September, October and November (mainly 360° to 180°).

4.1.4 Synthesis

The preliminary comparison with the offshore area revealed the importance of fresh runoffs to the salinity cycle observed at the LTER-MC point in the GoN, and the probable presence of horizontal advection mechanisms that partially modulate the offshore to inshore gradient and limit the exchanges of salt. The site displays a classic seasonal cycle for temperature with the start of stratification in March and the progressive deepening of thermocline to 20 m during spring-summer periods. By contrast salinity displays a time lag in its minimum in respect to the annual maxima of FW fluxes, highlighting the coastal character of the site, as also evidenced by the salinity values generally lower than the typical values of the Tyrrhenian sea [Napolitano et al., 2014]. The contribution of fresher water to the stratification is maximum in June-July, while that of temperature is in September, the latter weighting 8:1 in respect to the former. The influence of Tyrrhenian inflow is more evident from September to November, when a remarkable, progressively thickening salty layer with salinity values close to the annual maximum overlies the progressively thinning bottom layer of relative less salty water but under a fresher layer with salinity lowered by coastal inputs. This intrusion affects the vertical stability, creating the conditions for salt fingering below the surface layers, as shown and discussed in Kokoszka et al. [2021]. In autumn and winter, instabilities are instead driven by temperature over the mixed layer that progressively deepens from 10 to 40 m with the stable layer progressively squeezed until its final disappearance in February. However, reverse temperature gradients generate surface instabilities from October to February. In BC, the contribution of salty water to the stratification is maximum in June-July, while that of temperature is in September, with the latter weighting between 4:1 and 8:1 in respect to the former. From January to April, salinity dominates by contributing more than 50% to the BC index. The two indexes IS and BC characterize the whole water column stability and display a different temporal pattern: IS has a maximum in August, while BC includes internal water column instabilities and has its maximum centered on September-October.

4.2 Inter-annual variability between 2001 and 2019

4.2.1 Unfold the temperature and salinity: some specific periods that impact the heat and freshwater contents

We calculate monthly anomalies to the mean seasonal cycle for T and S, in the layers of interest defined by the LTER-MC protocol (surface, 2, 5, 10, 20, 30, 40, 50, 60 m deep). Results are presented in **Fig. 5, top**. The inter-annual variability is clearly visible, and the succession of warm/cold and fresh/salty years is obvious to identify. This general overview indicates two typologies of anomalies for the temperature, from $\pm0.5\,°C$ to $\pm1\,°C$ in a large part of the full water-column (e.g. warm in 2001, 2002, 2007, 2014, 2016, 2017, cold in 2004, 2006, 2012, or 2015), or intensified from $\pm1\,°C$ to $\pm2\,°C$ in more local layers (surface and sub-surface in 2002, 2004 and 2005, 2009, 2012 and 2018, or closer to the bottom at the end of 2010, 2015 and 2018). Salinity is marked too, with moderate anomalies from $\pm0.05\,\mathrm{g\,kg^{-1}}$ to $\pm0.15\,\mathrm{g\,kg^{-1}}$ distributed in the water-column (salty in 2001 to 2003, 2006, 2009, 2012 and 2013, 2016 and 2017, and fresh in 2002-2003, 2004, 2009 to 2011, 2014 and 2015, 2018), or above $\pm0.2\,\mathrm{g\,kg^{-1}}$ in localized layers (in surface, salty in 2002, 2003, 2005, 2009, 2017 and 2019, and fresh in 2004, 2010-2011, 2014, 2019).

These anomalies are integrated into the water-column budgets HC and FW, whose anomalies to their associated mean seasonal cycles are presented in **Fig. 6, bottom**, averaged by seasons year by years. Minimum anomalies of HC are visible during the following periods: spring in 2004, 2005 and 2006, summer in 2004, autumn 2011, and winter 2005 and 2015, with values close and above $-2\times10^8\,\mathrm{J\,m^{-2}}$. Moderate anomalies are visible too, from $-0.5\times10^8\,\mathrm{J\,m^{-2}}$ to $-1\times10^8\,\mathrm{J\,m^{-2}}$, during longer periods with successive seasons in 2009, 2011, 2012, spring and summer 2013, and in 2015. Positive anomalies are visible during the following periods: spring in 2001, 2002, 2007, 2014, 2016 to 2018, summer in 2002, 2007-2008, 2016 to 2019, autumn in 2010, 2013-2014, 2016, 2017-2018, and winter in 2006, 2008, 2013-2014, and 2019, with values close and above $2\times10^8\,\mathrm{J\,m^{-2}}$. Moderate anomalies are visible too, from $0.5\times10^8\,\mathrm{J\,m^{-2}}$ to $1\times10^8\,\mathrm{J\,m^{-2}}$, during longer periods in 2002, 2008, then at the end of 2013, 2014, 2016, and the first half of 2017, then in 2018 and 2019. In **Fig. 6, bottom** freshest years occur in 2004, 2007, 2009 to 2011, 2014 and early 2015 and late 2018, with anomalies values above 25 cm. Driest periods are the year 2001, the first semesters of 2002 and 2003, the years 2005, 2006, then 2016, 2017 and 2019, with negative values below -20 cm.

4.2.2 Inter-annual cycles : trends, modulations, and decadal variations

Thereafter we mention the period 2001-2009 as the decade I, and the period period 2010-2019 as the decade II. We show in the **Fig. 7** the inter-annual cycles of the quantities related to T and S, from in situ observations and ERA5. Both trends and modulations can be observed, illustrating the complexity of the thermal and saline contributions in such area. Linear trends are shown in the **Fig. 7** during the periods 2001-2019 (linear straight lines) and 2005-2019 (linear dashed lines). Values are summarized in the **Tab. 1** (all the estimates are available in supplementary files, see Supplementary Information). Regarding the surface temperature (**Fig. 7.a**), in situ and satellite indicate increasing trends of respectively $+0.01\,°C$/year and $+0.033\,°C$/year during the period 2005-2019. Note that the heatwave event that occurred over all Western Europe during the summer 2003 (Olita et al. [2007]) is visible here, and creates a negative slope if taken in account for the trend calculation. Bottom temperature follows a trend of $+0.03\,°C$/year (2005-2019) and exhibits a pseudo periodic modulation (from 3 to 5 years) in the same time than surface. This is visible too in the salinity and precipitations signals (**Fig. 7, right**), whose linear trends during 2005-2019 are $+0.002$ and $+0.006\,\mathrm{g\,kg^{-1}}$/year (surface and bottom salinity), and $+0.014\,\mathrm{mm\,d^{-1}}$/year for P-E. The modulation is repeated into the HC and FW index (that integrates the full water-column), but with weak linear trends ($+0.003\times10^9\,\mathrm{J\,m^{-2}}$/year and -0.548 cm/year, respectively, during 2005-2019).

We show then variability of IS and BC in **Fig. 7.e,f**, whose inter-annual trends reproduce the same modulations (their differences being mainly seasonal), except for IS during the period 2013 to 2015. Compared to BC, IS shows a weaker trend. This proxy does not take in account the water-column content, that leads to mark trends in the BC budget. In BC (**Fig. 7.f**), the total contribution of T and S (black line) shows a decreasing trend ($-0.12\,\mathrm{kg\,m^{-2}}$/year during 2001-2019), with a periodic modulation having a delayed phase of 1 to 2 years compared to HC during the decade I. Its thermal component (red line) follows the same modulation, and its decreasing trend is visible too ($-0.24\,\mathrm{kg\,m^{-2}}$/year during 2001-2019), compensated in BC by the increasing trend of the saline component ($+0.12\,\mathrm{kg\,m^{-2}}$/year during 2001-2019, in **Fig. 7.g**), that shows then a stronger contribution to the total BC during the decade II. Our interpretation is the following: even decreasing in intensity, the buoyancy is progressively reinforced in its saline component, stably ordered on the vertical dimension, i.e. relatively lighter (fresher) on surface and relatively heavy (salty) on bottom. This could be the signature of the horizontal advection of different water parcels, whose rates of exchange between coast and offshore could lead the general trend observed on BC. This is suggested in **Fig. 7.b**, with a strong change in surface salinity during the second decade, passing from values centered from $37.8\,\mathrm{g\,kg^{-1}}$ to $38.0\,\mathrm{g\,kg^{-1}}$ during the decade I, to values from $37.6\,\mathrm{g\,kg^{-1}}$ to $37.8\,\mathrm{g\,kg^{-1}}$ in decade II. We can note the year 2017, marked by a mean peak of $38.2\,\mathrm{g\,kg^{-1}}$, and particularly strong negative anomalies of FW during the whole year (as seen before), and that was the driest in terms of precipitations rates (**Fig. 7.i**). The bottom salinity shows a more limited dynamic compared to the surface, but exhibits and increasing trend during the second decade. All these variations are compensated into the FW index (**Fig. 7.d**), that in the same way than HC takes in account the full water-column, and consequently does not show such clear trends. The long term general variability observed in the inter-annual cycle of precipitations appears to impact the local content of salinity. P-E shows an increasing trend disrupted by groups of dry years (2001, 2006-2007, 2011, 2015-2016, 2017), but direct correspondence with salinity is rendered complex, probably due to the effect of horizontal advection of water masses at the coastal area, importing both fresh runoffs from the coast, and salty parcels from offshore. Finally, the inter-annual cycle of the surface fluxes (**Fig. 7.h**) reproduces well the increasing trend in the Mediterranean Sea as shown by Criado-Aldeanueva et al. [2012]. This macro driver is of interest as it describes the state of the large scale atmospherical forcings that applied to our regional area. Here we can describe its cycle by two periods, from low fluxes in decade I to higher fluxes in decade II. This descriptive framework will drive us then to the inter-annual cycle of seasons, when these trends have been stronger.

4.2.3 Impact on the mixed layer depth

The inter-annual mean values of $\mathrm{MLD}^{0.03}_{\sigma_0}$ (**Fig. 8**) identify 2007 as the year with the deepest mean MLD, nearly 32 m, while 2013, 2015 and 2019 are the years with the shallowest MLDs, with values lower than 19 m (**Tab. 2**). Also the cumulative of the stratified weeks displays a wide range of values (**Fig. 8, gray line**), with the shortest durations in 2002, 2003, 2007 and 2009 (from 26 to 29 weeks) and the longest ones in 2001, 2004-2005, 2011, 2013-2014, 2017 and 2019 (from 35 to 42 weeks, see **Tab. 2** and **Fig. 8**). Therefore changes in duration of stratification can go up to three months. The time series could be divided in groups of years displaying a long-term decadal trend interrupted by transition years, as we identify the two main periods I and II. Inside these two groups, various shortest periods can be identified. The periods 2001-2003 and 2004-2007 mark two deepening trends in the MLD, reflecting in the two decreasing trends seen in the cumulative of weeks. Then the period 2008-2011 shows a shallowing and an elongation of the cumulative, disrupted in 2012, and followed then by a more constant period in 2013-2015 with a relatively shallow MLD ($<$ 20 m) and long stratified periods (from 35 to 38 weeks). The final part of the time series recalls in some part its beginning from 2001 to 2003, with a deepening during 2016-2018 followed by some shallowing in 2019. The change in the cumulative of the stratified weeks follows a period of 3 to 5 years. The time course of the mixed layer displays a significant inter-annual variability with the initiation of the stratification fluctuating between March and April, and a progressive increase of its end in late autumn, with variations in the cumulative of stratified weeks up to three months. The maximum duration occurred in 2011 with 42 weeks, almost 80% of the whole year. In general, shallower ML tend to last longer while deeper ones tend to be shorter. The seasonal decomposition (**Fig. 8, bottom**) allows us to identify the autumnal cycle as the closest to the inter-annual cycle of the whole year, and winter is the season when the inter-annual trend and shift between decades are the most visible. It is noteworthy to point out that the spring cycle tends to present a moderate trend of deepening, with values below 15 m in 2003-2008, slightly shifting above 15 m during the decade II. Considering winters, the water-column can be qualified of 'fully mixed' ($\overline{\mathrm{MLD}}^{2001\text{-}2009}_{\mathrm{winter}} \approx 57.9m$) during the decade I, while the situation is rarer during the decade II ($\overline{\mathrm{MLD}}^{2010\text{-}2019}_{\mathrm{winter}} \approx 44.7m$).

4.2.4 Synthesis

Inter-annual variability is clearly visible with a succession of warm/cold and fresh/salty years. This general overview indicates two typologies of anomalies for both temperature and salinity, in a large part of the full water-column, and in more local layers (surface and sub-surface for T and S, or closer to the bottom for T). Various trends and modulations can be observed in the inter-annual series, illustrating the complexity of the thermal and saline contributions to the stratification in such area. In general surface and bottom (T, S, P-E, SST) shows trends between decades (**Tab. 1**), and remarkable modulations with a period from 3 to 5 years. Integrated quantities (HC, FW) exhibits weaker trends and modulations too, with various phases (BC delayed of 1 to 2 years compared to HC in the decade I). Comparing the two decades, we can see a strong change in the surface salinity, passing from values centered from $37.8\,\mathrm{g\,kg^{-1}}$ to $38.0\,\mathrm{g\,kg^{-1}}$ during the decade I, to values from $37.6\,\mathrm{g\,kg^{-1}}$ to $37.8\,\mathrm{g\,kg^{-1}}$ during the decade II. This indicates that water-columns budgets may not change (sensu of the trends for HC, FW), while stratification can increase or decrease (BC). The long term general variability observed into the inter-annual cycle of precipitations appears to impact the local content of salinity. P-E shows an increasing trend disrupted by groups of dry years, but direct correspondence with salinity is rendered complex ($+0.002\,\mathrm{g\,kg^{-1}}$/year during 2005-2019, but $-0.004\,\mathrm{g\,kg^{-1}}$/year if considering 2001-2019), probably due to the mitigating effect of horizontal advection in the coastal area, importing both fresh runoffs from the coast, and salty parcels from the offshore. The inter-annual cycle of the surface fluxes ($+0.74\,\mathrm{W\,m^{-2}}$/year for Q_{net} during 2001-2019) reproduces well the decadal variability observed in the Mediterranean Sea as shown by Criado-Aldeanueva et al. [2012]. We propose to describe the variability by two periods, from low fluxes during the decade I to higher fluxes during the decade II. During the whole period 2001-2019, linear trends are of $+3.82\times10^{-10}\,\mathrm{W\,kg^{-1}}$/year for BF, $+2.0\times10^{-6}\,\mathrm{m\,s^{-1}}$/year for u^*. In terms of proxy of the stratification, mean inter-annual values of $\mathrm{MLD}^{0.03}_{\sigma_0}$ indicates a shallowing of $-0.30\,\mathrm{m}$/year during the period 2001-2019 ($-0.53\,\mathrm{m}$/year if considering 2005-2019), progressively confined toward surface. Counting the weeks when the values are above 22 m, shortest cumulative ranges from 26 to 29 weeks, and longest from 35 to 42 weeks, showing an increasing trends of this 'duration' between the two main periods I and II. This long-term decade trend is interrupted by transition years, and the change in the cumulative exhibits the same modulations as observed in the thermal and saline drivers. When decomposing by seasons, the autumnal cycle is the closest to the inter-annual cycle of the whole year. A more moderate trend of deepening is visible in spring ($+0.14\,\mathrm{m}$/year during 2005-2019, see supplementary Tab. S1) with values below 15 m in 2003-2008, slightly shifting above 15 m during the 2010-2019 decade. Winter is the season when the inter-annual trend and shift between decades is the most visible: during winters of the decade I, the water-column can be considered 'fully mixed' ($\overline{\mathrm{MLD}}^{\text{2001-2009}}_{\text{winter}} \approx 57.9m$) , then the situation is rarer during the decade II ($\overline{\mathrm{MLD}}^{\text{2010-2019}}_{\text{winter}} \approx 44.7m$).

4.3 Inter-annual variability of the winter season

We identified the main drivers of the seasonal cycles, and the inter-annual modulations of the external forcing, such as rain and heat fluxes, with their impact on the in situ budgets of heat content and freshwater. We investigate here the consequences on the MLD itself. With such a signal in winter ($-1.27\,\mathrm{m/year}$ during the period 2001-2019), in the next part we focus on the inter-annual variability of the drivers during this season. We introduce estimates of the regional forcings, calculated from the bulk parameters extracted from the ERA5 data set (see Methods). To provide insights between mechanical and thermodynamical contributions to the deepening of the MLD, we use the wind and surface fluxes fields to infer the wind friction on surface (u_*) and the buoyancy fluxes (BF). The variability of the wind intensity is informative on the local vertical mixing processes, but here we investigate also the variability of the wind direction since the boundary effect due to the geographical embayment of the LTER-MC station could have an influence on the accumulation/export of fresh/salty water parcels. At the top of these quantities we describe the time series of the climatic indices of the NAO and WEMO (see Methods) as proxy of the atmospherical context driving the neighbour basins, and possibly influencing our regional area, as it has been shown to have a decadal impact on the northern part of the Mediterranean area [Bonifacio et al., 2019]. All of the mentioned variables during winter are presented in **Fig. 9** (the time series for all seasons can be consulted in the supplementary Fig. S2). Indices in **Fig. 9** reveal a shift to the Atlantic westerlies influence (i.e., positive NAO and WEMO) after 2010 that is particularly visible on winter seasons, while the WEMO index was quasi always negative during the decade I (i.e., steady dominant Mediterranean easterlies). When performing T-Test between two separated segments of the inter-annual winter series, to confirm statistically different regimes (e.g. here two decades), the best results are obtained when comparing the segments [2001-2009] and [2010-2018]. We obtain low p-values of 0.008 for MLD, 0.038 for ΔS (difference of surface salinity between the GoN and outside), 0.027 for u^*, 0.064 for NAO, 0.004 for WeMO, and moderately significant values of 0.206 and 0.234 for BF and the wind direction. This reinforces the situations we depicted previously about the two decadal periods I ans II, inside whom the interplay and dominance between drivers could have been different.

4.3.1 The hypothesis of a regime shift in winter after the transition of 2009-2010

The seasonal decomposition reveals an interesting variability, with a possible winter shift during after the transition of 2009-2010, suggesting an Atlantic influence over the Mediterranean area, possibly observable at the LTER-MC point. The regime shift between East-Mediterranean and West-Atlantic is visible on the wind trades (**Fig. 9**) showing the appearance of winds oriented toward the coast (below 150°, so orientated toward East to Northwest), marking a difference with the dominance of the wind oriented to the offshore during the decade I. In the wind, the inter-annual series is marked by a diminishing in the energy with the friction passing from around $5.5\times10^{-3}\,\mathrm{m\,s^{-1}}$ during the decade I, to around $4.8\times10^{-3}\,\mathrm{m\,s^{-1}}$ during II. We showed that the mixed layer can be limited in winter by the salty content, and this could be amplified by the increase in salt visible in **Fig. 9** during the decade II. Interestingly, during this period this signal seems to couple with the offshore salinity. This could be an indicator of favorized exchange with the open Tyrrhenian area in the horizontal import/export of inshore/offshore parcels. The increase in the convective BF is visible too, passing from low values from $-3\times10^{-8}\,\mathrm{W\,kg^{-1}}$ to $-4\times10^{-8}\,\mathrm{W\,kg^{-1}}$ before the mid 2010s, to larger values after.

4.3.2 Investigation of the mixed layer depth's drivers

4.3.2.1 Two different regimes in winter in functions of the wind and the buoyancy fluxes The winter trends revealed a remarkable relationship between the MLD and the wind stress during the two decades. In **Fig. 10** a linear trend is visible between averaged $\overline{MLD}$ and $\overline{u_*}$ during the decade II. Decade II shows a linear control, low/high stress associated to a shallow/deep MLD regime, not visible during the decade I. Interestingly, decade I indicates a cluster of deep MLD (> 50 m) associated with intense low BF ($< -3\times10^{-8}\,\mathrm{W\,kg^{-1}}$), while decade II suggest a more linear distribution. In terms of wind direction, decade I indicates dominant directions centered on around 220° (blowing toward the South-West quarter, i.e. in direction of the offshore), while the decade II shows more variance with directions spreading widely toward the North direction (i.e. blowing in direction of the coast). About the inshore-offshore gradient of salinity in surface, deep values of MLD are associated with the largest and positive differences beween the GoN and the Tyrrhenian area (i.e. GoN relatively saltier), while the decade II shows an increasing coupling with the open area, with differences diminishing toward zero, or being negative (i.e. GoN relatively fresher). Due to presence of mesoscale features all the year long, we hypothesize that a coupled configuration would be favorable to express the influence of such structures inside the GoN by redistributing fresh/salty parcels during the decade II.

4.3.2.2 Relative contributions of the selected drivers to the MLD's modelization To go further and extend this analysis to the other seasons when the trends of the MLD are less marked (i.e. spring and autumn), we perform a random forest regression to assess the individual weights of the various contributors to the MLD (see Methods). We aim to modelize the in situ MLD in function of independent external parameters (i.e. external data set such as provided by Copernicus, like ERA5). To this, we hypothesize that large-scale atmospherical conditions (sensu climate indices NAO or WEMO) could have led to different dynamical regimes, i.e. thermodynamical (e.g. convective fluxes) and mechanical (e.g. wind stress) forcing could have varied in their dominance and timing. To distinguish between some possible cases, the regression tree has been trained by subsets, splitting the time series by seasons and decades I and II, trying to reproduce the observations of the MLD with the help of predictors. The importance of the predictors are shown in **Fig. 11**, aside from the scatter plots of the MLD predicted by each training. Performance values are presented in the **Tab. 3**. The regression performed better for the decade I (correlation of 0.89) compared to the decade II (0.75). In general, when compared to observations, the mean error between prediction and validation data is lower than if using an atlas value (i.e. using the 2001-2019 monthly averages of MLD): we improve the estimate when using the prediction. When looking at seasons individually by decades, the training assimilation of the winter I was more difficult, with a fit whose quality performs less better (p-value 0.12) than for the winter II (significant p-value 0.00174). In spring and autumn a better performance is obtained in predicting the MLD, and for both decades the errors are reduced when using the prediction instead of the atlas. Keeping apart the limitations, especially for the winter II, we show the good performance of the method. Even if the results in winter have to be considered with care, we briefly describe them here for sake of completeness. During the decade I, a dominant importance is given by the wind direction (more than 20%), while during decade II that role is given to BF (more than 30%). BF are more stabilizing during this decade, with the general tendency of heat increase, and, as suggested before, this reinforces the hypothesis that more possibility is given to the wind stress in the role of mixing the surface layer. To resume: the situation of deep MLD (decade I) could be set by the consistent wind direction aligned toward the offshore (dilution of coastal fresh runoffs), and strong convective BF, helped secondarily by the intermittent wind events. Then the situation of shallow MLD (decade II) could results from a change in the wind direction retaining fresh water parcels close to the coast, a more stable BF, and a wind stress controlling linearly the deepening of the MLD given the more stable configuration. This situation could be repeated in spring during the decade II: P-E passes from 10 to 20%, and the wind stress from 5 to 20%. This interpretation could be applied to the autumn too, with more importance given to the SST (more than 30%), whose increase could matter to the shallowing tendency of the MLD. This could set the stable configuration, against which the wind stress (importance increasing from 5 to 10% between decade I and II) could express its linear control of the deepening, as in the winter configuration.

4.3.3 Synthesis

We characterized the atmospherical context. Two opposite trends in the surface fluxes are visible during the quasi bi-decadal period, while NAO and WEMO indices suggest a regime shift that happened in winter after the years 2009-2010. The regime shift is visible through wind trades, shifting from the easterlies dominance during the decade I, to the appearance of westerlies components during the decade II. Decade II is marked by a diminishing in the energy with the wind stress, higher BF (i.e. less destabilizing), and more spread winds toward the coast, and more coupling with the offshore in terms of salinity. Decade I is marked by lower BF (i.e. more destabilizing), winds oriented toward the offshore, and less coupling with the offshore in terms of salinity. As shown by the inter-annual seasonal decomposition of the MLD, the main inter-annual shallowing trend is mostly visible during in the Dec.-Feb. season (winter), and reproduced secondarily in the Sep.-Nov. season (autumn), while Mar.-May (spring) shows a slight deepening trend. When related to the MLD, the remarkable linear trends that oppose between the two decades suggest a situation dominated by the BF in decade I, and by the wind in decade II. During the decade II, the mechanical mixing due to wind could express more linearly than in the decade I, due to the stabilizing effect of the import of fresh parcels by the horizontal circulation (e.g. mesoscale).

5 Discussion

Our detailed analysis of the 2001-2019 time series of temperature and salinity at the LTER-MC station allowed us to extend and complete the former study by Ribera d'Alcala et al. [2004] by characterizing the relative importance of the main drivers of the water column dynamics for this specific site over the two decades. This creates an appropriate framework to formulate hypotheses on the impact of predicted climate changes on the area and to depict possible scenarios with which plankton communities should scope in the near future. The link between plankton dynamics at the site and the water column structure is the subject of an ongoing analysis which necessitated the work presented here.

5.1 Overview of this coastal area : classic in temperature, specific in salinity, both subjects to seasonal and inter-annual trends

The climatological pattern at the site displays a classic seasonal cycle for temperature (minimum in February-March, maximum in July-August), whose inter-annual trend follows the warming trend inferred from the satellite observations on temperature surface, locally or over the whole Mediterranean basin since the mid 2010s [Iona et al., 2018]. This increasing trend and its overlap with a modulation of multi-annual periods, from 3 to 5 years, will be discussed thereafter. This impacts both surface and bottom depths, making linear trend less visible as we consider the full water-column instead of surface only. This shows that warming impacted the full water-column in such a shallow area, where variability is marked by the oscillating multi-annual modulations, without showing a clear net increase (or decrease) during the period considered. This suggests the need for longer consistent monitoring to identify more significant linear trends.

Salinity also plays an important role in the water column stability via the establishment of the surface freshwater layer in spring and of the salty water layer at mid-depth in September-November. This saltier water is an intrusion of offshore water, marking a specific dependency of this coastal site to the regional ocean circulation. Because of this intrusion the water column divides in three layers, with salinity maximum and intermediate temperature which promote double diffusion with the surface and the bottom layer, as shown in the study by Kokoszka et al. [2021] that highlighted the presence and persistence of density staircases below the MLD at this moment of the year. This could have an effect on the MLD itself, as it stabilizes the surface layer, and could drive the prolongation of the stratified period longer in the season, as it will be discussed thereafter. The maximum of freshwater input occurs before the salinity minimum since it is masked by the vertical mixing in later winter. Moreover, this creates the condition of a barrier layer (Kara et al. [2000], Vissa et al. [2013]), leading to an overestimation of the MLD if inferred from temperature profiles instead of density, that includes this haline contribution. This salty water type results from the summer evaporation occurring in the Tyrrhenian sea or in outer part of the Gulf, since the surface layer at the site is, for most of time, fresher than the water underneath, because of the inputs from the coast, or because of fresh water advected from the close Sarno river [Cianelli et al., 2012, 2017], or from the neighboring Gulf of Gaeta [Iermano et al., 2012]. Considering the surface, the preliminary comparison with the offshore area revealed the importance of fresh runoffs effects on the salinity cycle as observed at the LTER-MC point in the GoN, having its minimum in May-June, one month later than the offshore, and two months later than the annual maxima of fresh water inputs occurring in February-March. This is also evidenced through the salinity values which are generally lower than the typical values of the Tyrrhenian sea [Napolitano et al., 2014].

This reveals the influence of fresh water content on coastal character of the site spanning over a longer time than the regional inputs, and suggests the presence of horizontal advection mechanisms that mitigate the offshore/inshore salty exchanges [Iermano et al., 2012, Cianelli et al., 2015]. From this simple climatological cycle, we assume a complex interplay between vertical processes and variable horizontal inputs, since the stratification at the site does not simply result from the strict local atmospheric forcing, heat and momentum fluxes, and precipitation, but is significantly impacted by land inputs on one hand and coupling with larger scale circulation on the other.

5.2 What do we learn from the trends we can observe at the coastal area ?

The inter-annual cycle of the surface fluxes reproduces the decadal variability observed in the Mediterranean Sea well, with the increasing trend initiated from the mid 2010's shown in Criado-Aldeanueva et al. [2012]. We can identify two cycles within its cycle, from low fluxes between 2001-2009, to higher fluxes between 2010-2019. In terms of atmospheric context, two opposite trends are visible in the surface fluxes, during a quasi bi-decadal period, while NAO and WEMO indices suggest a regime shift in the winter seasons after the years 2009-2010 [Bonifacio et al., 2019]. This could have led to a different interplay between wind and convective forcings, that we will discuss thereafter. We show that, even while being in a shallow coastal area, the site is not only influenced by local land inputs (fresh runoffs), but also by basin-scale drivers whose differentiation is rendered complex by the combination of their multi-decadal and decadal variabilities, as shown and discussed by [Parker et al., 2007], or more recently, the work of J. Zhang et al. [2020] on the North Atlantic multidecadal variability in the mid-high latitude. In our study, we pave the way to a better understanding of such interactions in the Tyrrhenian and Mediterranean Sea that could impact the coastal marine ecosystems services of the GoN.

More locally, we showed that the main driver of the fresh water budget is precipitation, directly and indirectly, which has significantly more impact than evaporation. It implies that long term changes are also possibly impacted by the effects of climate change on the surrounding territories, which include regions with important winter snow accumulations (note the proximity of Mount Vesuvius, in the northern part of the gulf, and the Monti Lattari in its southeastern part, these mountain systems having altitudes higher than 1200 m). However it is not just the local precipitation, i.e., that directly falls in the Gulf, but also those conveyed to the GoN via the catchment area land side of the Gulf that contribute. Note that without measurements of the river runoffs contribution, they were not accounted for despite the fact that they are likely important over this coastal area (the Sarno river runoff into the Gulf of Naples is about 13 $m^3\,s^{-1}$, while the Volturno river runoff into the Gulf of Gaeta is about 82 $m^3\,s^{-1}$, from Albanese et al. [2012]). Further stratification enhancement derives from the contrast between a fresher surface layer and saltier layer underneath which is very seldom interrupted by events of flushing by offshore waters *(pinpoint)* which reinforces the prolongation of the stratified period and the tendency toward a shallower MLD over the years. In a context of rising air and sea temperatures, and of intensifying extreme events such as storms, floods and even, recently, Mediterranean hurricanes, the fresh water influence becomes a primer in such regional area surrounded by land and mountains [Volosciuk et al., 2016, Koseki et al., 2020, W. Zhang et al., 2020].

The system being fresher and more stratified, it then raises the question of its connectivity to the offshore. Interestingly, the seasonal decomposition and comparison with the neighbouring Tyrrhenian Sea during winter suggested an enhanced coupling between offshore and embayment during the decade 2010-2019. It remains to determine if such coupling was facilitated by a shallower winter MLD (i.e. more stratified situations) that promoted horizontal exchanges between the gulf and the open area. Contribution of mesoscale through water parcels mixing and advection remains to be investigated. The seasonality associated to the mesoscale may be different from the seasonality of external drivers, the vortices structures being present all year long [Fernandez et al., 2005, Bonaduce et al., 2021], while submesoscale flows can be expected to be much stronger in winter than in summer [Callies et al., 2015]. The role of submesoscale, considered here as the formation of filaments, depends also on the runoff input of high potential vorticity (maximal in spring and early summer) and in general from anomalies in the stratification. An enhanced coupling between the internal/external areas during the decade 2010-2019 could have then promoted trade-offs driven by such structures, whose role on the redistribution of the water parcels (fresh or salty) inside the Gulf remains to be determined.

5.3 MLD : a proxy of the stratification resulting from interplaying processes

The MLD, taken as a proxy of the stratification, evolved over years, while the macro indexes (intensity of the stratification, and buoyancy anomaly content) neither reflected the same evolution. Even if marked by the periodic modulations discussed before, the inter-annual average of the MLD shows a remarkable trend in its shallowing. The MLD is progressively confined towards the surface, and this is coupled with a lengthening in the cumulative of the stratified weeks over the quasi 20 year time span (from shortest between 26 to 29 weeks, to longest from 35 to 42 weeks). The inter-annual variations show an increasing trend of this 'duration', between two main periods 2001-2009 and 2010-2019. This long-term decade trend is interrupted by transition years, and the change in the cumulative shows the same modulations as those observed in the thermal and saline drivers.

When decomposing by seasons, we identify that the autumnal cycle is the closest to inter-annual cycle of the whole year, while a moderate trend of deepening is visible in spring with values above 15 m during the second decade. This may be due to salinity which contributes 50% more than temperature to buoyancy content in general from January to April (situation of cold waters with salty parcels in the water-column, remaining from the winter period). Winter is the season when the inter-annual trend is the most visible, with a remarkable shift between the two decades 2001-2009 and 2010-2019, the water-column possibly being considered 'fully mixed' during the decade I, followed by a rare situation during the decade II. As shown by Zingone et al. [2010], this period is of importance for the physical and biological marine ecosystem of the Gulf of Naples, as it sometimes reproduces (prolongates) the late-summer nutrients-rich conditions, and primes the primary production for the next spring.

We present here our hypothesis about the ML control: accumulating freshwater in a salty arena and disrupting it with the wind. We propose here a speculative scheme about the fresh runoff inter-playing with wind forcing on the surface layer, from the end of summer to the heart of winter. Under easterlies conditions (e.g. dominant regime suggested during 2001-2009), the river fresh water output can be exported offshore and diluted within the ambient salty water, leading to the classic scheme of a ML extending to the bottom, controlled primarily by destabilizing convection and wind. Shifting the wind regime to westerlies (e.g. suggested during 2010-2019), and considering the barrier made by the coast on which the continuous river discharge takes place, the situation could lead to an accumulation of fresh water at the coast, as it has been suggested by Cianelli et al. [2017]. This amount of water could inhibit the convective processes and limit the mixed layer to shallow depths compared to the previous case involving easterlies. With less destabilizing convective fluxes, the control could be done by the wind, as suggested by our inter-annual analysis of winter. In this context, the timing of intense wind events could be a primer, by disrupting the stable state intermittently and mixing the water-column. This could explain the elongation of the stratified period as observed during the 2010-2019 autumnal periods, with the conjunction of westerlies components in the wind direction, late storm events, and fresh water load into the system through the precipitation.

5.4 The GoN as a monitoring area of both physical and biological changes

When considering the Gulf of Naples in full, our study highlights the complexity of the ocean circulation reflected in the coastal observations, as it was recently pointed in the work of de Ruggiero et al. [2020] that assessed the dynamics of the area during a specific year (2016). The GoN is subject to various connectivity between its inner areas, and those that remain to be identified precisely to assess the impact on dynamic and variability of the biological communities. For this, a study on lagrangian studies, dedicated to follow chosen particles inputs (e.g. nutrients and pollutants discharge from the Sarno river, coastal runoffs from particular hotspots, or oligotrophic offshore waters) using ocean drifters and trajectories in numerical model, should be done in future studies. This would better answer the question on coupling between physics and biology when the coastal system experiences long-term trends, inter-annual modulations and extreme events : what are the biological responses to such stresses (or opportunities) for the ecosystem communities ?

In the context of climate change, we expect that the Mediterranean basin would go through an increase in fresh inputs (E-P) [Alpert et al., 2013], with heat waves occurring intermittently [Darmaraki et al., 2019, Holbrook et al., 2020]. This would cause an increase in salinity [Skliris et al., 2018] with a parallel increase in density, very weakly compensated by the increase in temperature. Accurate knowledge of the horizontal salinity field and wind stress are required to correctly determine the onset and breakdown of stratification [Ruiz-Castillo et al., 2019]. The local state of the surface layer is of importance here, as is the interplay with remote factor such as basins scale climate indices (i.e. NAO and WEMO), like timing and intensity of wind events have been shown to be controlled by larger scale features. In this case, a regime shift could impact the configuration of important parameters like wind, and consequently its directional forcing on the coastal system. More stratification leads to inhibited exchanges between the internal layers of the water column and the atmosphere, but promotes internal wave activity [Woodson, 2018], changing the way nearshore ecosystems are exposed to deep offshore waters. The present study of the long term time series, from CTD observations obtained with a consistent effort – but nevertheless relatively simple, shows the importance, as pointed recently by [Bonifacio et al., 2019], to accumulate and build regional climate indexes. It proposes a step forward to the constitution of an index and atlas for future studies, that could strengthen the predictability of the marine coastal ecosystems with the joint contributions of numerical simulations, machine learning, and comparisons to in situ observations.

References

Adloff, F., Somot, S., Sevault, F., Jordà, G., Aznar, R., Déqué, M., ... Gomis Bosch, D. (2015, 02). Mediterranean sea response to climate change in an ensemble of twenty first century scenarios. *Climate Dynamics*, *2507*, 1-28. doi: 10.1007/s00382-015-2507-3

Albanese, S., Iavazzo, P., Adamo, P., Lima, A., & De Vivo, B. (2012, 09). Assessment of the environmental conditions of the sarno river basin (south italy): A stream sediment approach. *Environmental Geochemistry and Health*, *35*. doi: 10.1007/s10653-012-9483-x

Alpert, P., Hemming, D., Jin, F., Kay, G., Kitoh, A., & Mariotti, A. (2013). The hydrological cycle of the mediterranean. In A. Navarra & L. Tubiana (Eds.), *Regional assessment of climate change in the mediterranean* (Vol. 50, pp. 201–239). Springer.

Behrenfeld, M. J. (2010). Abandoning sverdrup's critical depth hypothesis on phytoplankton blooms. *Ecology*, *91*(4), 977–989.

Bethoux, J., Gentili, B., & Tailliez, D. (1998, 04). Warming and freshwater budget change in the mediterranean since the 1940s, their possible relation to the greenhouse effect. *Geophysical Research Letters*, *25*, 1023-1026. doi: 10.1029/98GL00724

Bonaduce, A., Cipollone, A., Johannessen, J. A., Staneva, J., Raj, R. P., & Aydogdu, A. (2021). Ocean mesoscale variability: A case study on the mediterranean sea from a re-analysis perspective. *Frontiers in Earth Science*, *9*. doi: 10.3389/feart.2021.724879

Bonifacio, P., Grémare, A., Amouroux, J.-M., & Labrune, C. (2019, 08). open-access: Climate-driven changes in macrobenthic communities in the mediterranean sea: A 10-year study in the bay of banyuls-sur-mer. *Ecology and Evolution*. doi: 10.1002/ece3.5569

Breiman, L. (2001, 10). Machine learning, volume 45, number 1 - springerlink. *Machine Learning*, *45*, 5-32. doi: 10.1023/A:1010933404324

(C3S), C. C. C. S. (2017). Era5: Fifth generation of ecmwf atmospheric reanalyses of the global climate. *Copernicus Climate Change Service Climate Data Store (CDS), date of access*. doi: https://cds.climate.copernicus.eu/cdsapp#!/home

Callies, J., Ferrari, R., Klymak, J., & Gula, J. (2015, 04). Seasonality in submesoscale turbulence. *Nature Communications*, *6*, 6862. doi: 10.1038/ncomms7862

Cianelli, D., D'Alelio, D., Uttieri, M., Sarno, D., Zingone, A., Zambianchi, E., & Ribera d'Alcala, M. (2017, 12). Disentangling physical and biological drivers of phytoplankton dynamics in a coastal system. *Scientific Reports*, *7*. doi: 10.1038/s41598-017-15880-x

Cianelli, D., Falco, P., Iermano, I., Mozzillo, P., Uttieri, M., Buonocore, B., ... Zambianchi, E. (2015, 01). Inshore/offshore water exchange in the gulf of naples. *Journal of Marine Systems*. doi: 10.1016/j.jmarsys.2015.01.002

Cianelli, D., Uttieri, M., Buonocore, B., Falco, P., Zambardino, G., & Zambianchi, E. (2012, 08). Dynamics of a very special mediterranean coastal area: the gulf of naples. *Mediterranean Ecosystems: Dynamics, Management and Conservation*, 129–150.

Criado-Aldeanueva, F., Soto-Navarro, F. J., & García-Lafuente, J. (2012). Seasonal and interannual variability of surface heat and freshwater fluxes in the mediterranean sea: budgets and exchange through the strait of gibraltar. *International Journal of Climatology*, *32*(2), 286-302. doi: https://doi.org/10.1002/joc.2268

Darmaraki, S., Somot, S., Sevault, F., Nabat, P., Cabos Narvaez, W. D., Cavicchia, L., ... Sein, D. (2019, 08). Future evolution of marine heatwaves in the mediterranean sea. *Climate Dynamics*, *53*. doi: 10.1007/s00382-019-04661-z

de Boyer Montégut, C., Madec, G., Fischer, A. S., Lazar, A., & Iudicone, D. (2004).

Mixed layer depth over the global ocean: An examination of profile data and a profile-based climatology. *Journal of Geophysical Research: Oceans*, *109*(C12).

de Ruggiero, P., Esposito, G., Ernesto, N., Iacono, R., Pierini, S., & Zambianchi, E. (2020, 05). Modelling the marine circulation of the campania coastal system (tyrrhenian sea) for the year 2016: Analysis of the dynamics. *Journal of Marine Systems*, *210*, 103388. doi: 10.1016/j.jmarsys.2020.103388

El Hourany, R., Mejia, C., Faour, G., Crépon, M., & Thiria, S. (2021, 04). Evidencing the impact of climate change on the phytoplankton community of the mediterranean sea through a bioregionalization approach. *Journal of Geophysical Research: Oceans*, *126*. doi: 10.1029/2020JC016808

Escudier, C. E. O. M. C. A. P. J. A. A. D. M. G. A. L. V. L. R. C. S. M. S. C. G. . P. N., R. (2020). Mediterranean sea physical reanalysis (cmems med-currents) (version 1) set. *Copernicus Monitoring Environment Marine Service (CMEMS).* doi: doi.org/10.25423/CMCC/MEDSEA_MULTIYEAR_PHY_006_004_E3R1

Fernandez, V., Dietrich, D., Haney, R., & Tintoré, J. (2005, 08). Mesoscale, seasonal and interannual variability in the mediterranean sea using a numerical ocean model. *Progress In Oceanography*, *66*, 321-340. doi: 10.1016/j.pocean.2004.07.010

Ferrari, R., & Wunsch, C. (2009). Ocean circulation kinetic energy: Reservoirs, sources, and sinks. *Annual Review of Fluid Mechanics*, *41*, 253–282.

Frontier, S., Pichod-Viale, D., Leprêtre, A., Davoult, D., & Luczak, C. (2008). *Ecosystèmes. structure, fonctionnement, évolution.* Dunod, Paris.

GEBCO, C. G. (2020). *Gebco 2020 grid.* Retrieved from `https://www.gebco.net` doi: 10.5285/a29c5465-b138-234d-e053-6c86abc040b9

Giorgi, F. (2006, 04). Climate change hot-spots. *Geophysical Research Letters*, *33doi*, 101029/. doi: 10.1029/2006GL025734

Giorgi, F., & Lionello, P. (2007, 10). Climate change projections for the mediterranean region. *Global and Planetary Change*, *63*, 90-104. doi: 10.1016/j.gloplacha.2007.09.005

Guancheng, l., Cheng, L., Zhu, J., Trenberth, K., Mann, M., & Abraham, J. (2020, 12). Increasing ocean stratification over the past half-century. *Nature Climate Change*, *10*, 1-8. doi: 10.1038/s41558-020-00918-2

Hallett, C., Hobday, A., Tweedley, J., Thompson, P., Mcmahon, K., & Valesini, F. (2018, 06). Observed and predicted impacts of climate change on the estuaries of south-western australia, a mediterranean climate region. *Regional Environmental Change*, *18*. doi: 10.1007/s10113-017-1264-8

Holbrook, N., Gupta, A., Oliver, E., Hobday, A., Benthuysen, J., Scannell, H., ... Wernberg, T. (2020, 07). Keeping pace with marine heatwaves. *Nature Reviews Earth Environment*, *1*. doi: 10.1038/s43017-020-0068-4

Hurrell, J. W. (1995). Decadal trends in the north atlantic oscillation: Regional temperatures and precipitation. *Science*, *269*, 676–679. doi: doi.org/10.1126/science.269.5224.676

Hurrell, J. W., & Deser, C. (2009). North atlantic climate variability: The role of the north atlantic oscillation. journal of marine systems. *Journal of Marine Systems*, *78*, 28–41. doi: doi.org/10.1016/j.jmarsys.2008.11.026

Iermano, I., Liguori, G., Iudicone, D., Buongiorno Nardelli, B., Colella, S., Zingone, A., ... Ribera d'Alcalà, M. (2012). Filament formation and evolution in buoyant coastal waters: Observation and modelling. *Progress in Oceanography*, *106*, 118-137. doi: 10.1016/j.pocean.2012.08.003

Iona, A., Theodorou, A., Sofianos, S., Watelet, S., Troupin, C., & Beckers, J.-M. (2018). Mediterranean sea climatic indices: monitoring long-term variability and climate changes. *Earth System Science Data*, *10*(4), 1829–1842. doi: 10.5194/essd-10-1829-2018

Kara, A., Rochford, P., & Hurlburt, H. (2000, 07). Mixed layer depth variability and barrier layer formation over the north pacific ocean. *Journal of Geophysical Research*, *105*. doi: 10.1029/2000JC900071

Kersalé, M., Petrenko, A. A., Doglioli, A. M., Dekeyser, I., & Nencioli, F. (2013). Physical characteristics and dynamics of the coastal eddy derived from in situ data and numerical modeling. *Journal of Geophysical Research: Oceans*, *118*(1), 399-409. doi: 10.1029/2012JC008229

Kokoszka, F., Iudicone, D., Zingone, A., Saggiomo, V., Ribera D'Alcalá, M., & Conversano, F. (2021, 12). A note about density staircases in the gulf of naples : 20 years of persistent weak salt-fingering layers in a coastal area. *Advances in Oceanography and Limnology*, *12*(2). doi: 10.4081/aiol.2021.10008

Koseki, S., Mooney, P., Cabos Narvaez, W. D., Gaertner, m., de la Vara, A., & Aleman, J. (2020, 07). Modelling a tropical-like cyclone in the mediterranean sea under present and warmer climate. *Natural Hazards and Earth System Sciences*. doi: 10.5194/nhess-2020-187

Large, W., & Pond, S. (1981, 01). Open ocean momentum flux measurement in moderate to strong winds. *Journal of Physical Oceanography*, *11*, 336-342.

Lentz, S. (2012). Buoyant coastal currents. In C. Eric P., C. Claudia, & V. Jacques (Eds.), *Buoyancy-driven flows* (pp. 164–202). Cambridge University Press.

Margalef, R. (1978). Life-forms of phytoplankton as survival alternatives in an unstable environment. *Oceanologica acta*, *1*(4), 493–509.

Mariotti, A., Struglia, M. V., Zeng, N., & Lau, K. (2002). The hydrological cycle in the mediterranean region and implications for the water budget of the mediterranean sea. *Journal of climate*, *15*(13), 1674–1690.

Martin-Vide, . L. J. A., J. (2006). The western mediterranean oscillation and rainfall in the iberian peninsula. *International Journal of Climatology*, *26*, 1455–1475. doi: doi.org/10.1002/joc.1388

McDougall, T. J., & Barker, P. M. (2011). Getting started with teos-10 and the gibbs seawater (gsw) oceanographic toolbox. *SCOR/IAPSO WG*, *127*, 1–28.

Napolitano, E., Iacono, R., & Marullo, S. (2014). The 2009 surface and intermediate circulation of the tyrrhenian sea as assessed by an operational model. In G. L. Eusebi Borzelli, M. Gacic, P. Lionello, & P. Malanotte-Rizzoli (Eds.), *The mediterranean sea: temporal variability and spatial patterns, geophysical monograph* (Vol. 202, pp. 59–74). American Geophysical Union.

Olita, A., Sorgente, R., Natale, S., Gaberšek, S., Ribotti, A., Bonanno, A., & Patti, B. (2007). Effects of the 2003 european heatwave on the central mediterranean sea: surface fluxes and the dynamical response. *Ocean Science*, *3*(2), 273–289. doi: 10.5194/os-3-273-2007

Parker, D., Folland, C., Scaife, A., Knight, J., Colman, A., Baines, P., & Dong, B. (2007, 09). Decadal to multidecadal variability and the climate change background. *Journal of Geophysical Research*, *112*. doi: 10.1029/2007JD008411

Pedregosa, F., Varoquaux, G., Gramfort, A., Michel, V., Thirion, B., Grisel, O., ... Duchesnay, E. (2011). Scikit-learn: Machine learning in Python. *Journal of Machine Learning Research*, *12*, 2825–2830.

Ribera d'Alcala, M., Conversano, F., Corato, F., Licandro, P., Mangoni, O., Marino, D., ... Zingone, A. (2004, 04). Seasonal patterns in plankton communities in pluriannual time series at a coastal mediterranean site (gulf of naples): An attempt to discern recurrences and trends. *Scientia Marina*, *68*, 65–83.

Ruiz-Castillo, E., Sharples, J., & Hopkins, J. (2019, 11). Wind-driven strain extends seasonal stratification. *Geophysical Research Letters*, *46*. doi: 10.1029/2019GL084540

Sallée, J.-b., Pellichero, V., Akhoudas, C. H., Pauthenet, E., Vignes, L., Schmidtko, S., ... Kuusela, M. (2021, 03). Summertime increases in upper-ocean stratification and mixed-layer depth. *Nature*, *591*, 592-598. doi: 10.1038/s41586-021-03303-x

Sherman, K., Belkin, I. M., Friedland, K. D., O'Reilly, J., & Hyde, K. (2009). Accelerated warming and emergent trends in fisheries biomass yields of the world's large marine ecosystems. *AMBIO: a Journal of the Human Environment*, *38*(4), 215–224.

Skliris, N., Zika, J., Herold, L., Josey, S., & Marsh, R. (2018). Mediterranean sea water budget long-term trend inferred from salinity observations. *Climate Dynamics*, *51*(7-8), 2857–2876.

Smetacek, V., & Passow, U. (1990). Spring bloom initiation and sverdrup's critical-depth model. *Limnology and oceanography*, *35*(1), 228–234.

Smith, S. V., Buddemeier, R. W., Wulff, F., Swaney, D. P., Camacho-Ibar, V. F., David, L. T., ... others (2005). C, n, p fluxes in the coastal zone. In *Coastal fluxes in the anthropocene* (pp. 95–143). Springer.

Sverdrup, H. (1953). On conditions for the vernal blooming of phytoplankton. *Journal du Conseil / Conseil Permanent International pour l'Exploration de la Mer*, *18*(3), 287–295.

Truong, C., Oudre, L., & Vayatis, N. (2020). Selective review of offline change point detection methods. *Signal Processing*, *167*, 107299. doi: https://doi.org/10.1016/j.sigpro.2019.107299

Virtanen, P., Gommers, R., Oliphant, T. E., Haberland, M., Reddy, T., Cournapeau, D., ... SciPy 1.0 Contributors (2020). SciPy 1.0: Fundamental Algorithms for Scientific Computing in Python. *Nature Methods*, *17*, 261–272. doi: 10.1038/s41592-019-0686-2

Vissa, N. K., Satyanarayana, A. N. V., & Prasad Kumar, B. (2013). Comparison of mixed layer depth and barrier layer thickness for the indian ocean using two different climatologies. *International Journal of Climatology*, *33*(13), 2855-2870. doi: https://doi.org/10.1002/joc.3635

Volosciuk, C., Maraun, D., Semenov, V. A., Tilinina, N., Gulev, S. K., , & Latif, M. (2016). Rising mediterranean sea surface temperatures amplify extreme summer precipitation in central europe. *Scientific Reports*, *6*(32450). doi: 10.1038/srep32450

Walsh, J. J. (1988). *On the nature of continental shelves.* Academic Press, San Diego (CA), USA.

Woodson, C. (2018, 01). The fate and impact of internal waves in nearshore ecosystems. *Annual Review of Marine Science*, *10*. doi: 10.1146/annurev-marine-121916-063619

WTO. (2018). *World trade statistical review* (Tech. Rep.). World Trade Organization.

Xiu, P., Chai, F., Curchitser, E., & Castruccio, F. (2018, 02). Future changes in coastal upwelling ecosystems with global warming: The case of the california current system. *Scientific Reports*, *8*. doi: 10.1038/s41598-018-21247-7

Zhang, H.-M., & Talley, L. (1998, 10). Heat and buoyancy budgets and mixing rates in the upper thermocline of the indian and global oceans. *Journal of Physical Oceanography*, *28*, 1961–1978. doi: 10.1175/1520-0485(1998)028⟨1961:HABBAM⟩2.0.CO;2

Zhang, J., Chen, Z., Chen, H., Ma, Q., & Teshome, A. (2020, 04). North atlantic multidecadal variability enhancing decadal extratropical extremes in boreal late summer in the early 21st century. *Journal of Climate*, *33*, 6047-6064. doi: 10.1175/JCLI-D-19-0536.1

Zhang, W., Villarini, G., Scoccimarro, E., & Napolitano, F. (2020, 05). Examining the precipitation associated with medicanes in the high-resolution era-5 reanalysis data. *International Journal of Climatology*. doi: 10.1002/joc.6669

Zingone, A., Dubroca, L., Iudicone, D., Margiotta, F., Corato, F., d'Alcalà, M., ... Sarno, D. (2010). Coastal phytoplankton do not rest in winter. *Estuaries and Coasts*, *33*(2), 342-361. doi: 10.1007/s12237-009-9157-9

6 Tables

	Period [2005-2019] Linear trends / year	***Period [2001-2019]*** Linear trends / year
LTER-MC		
MLD	$-0.53\,\mathrm{m}$	$-0.30\,\mathrm{m}$
MLD winter	$-1.29\,\mathrm{m}$	$-1.27\,\mathrm{m}$
$\mathrm{T_{surface}}$	$+0.01\,°\mathrm{C}$	$-0.015\,°\mathrm{C}$
$\mathrm{T_{bottom}}$	$+0.03\,°\mathrm{C}$	$+0.008\,°\mathrm{C}$
$\mathrm{S_{surface}}$	$+0.002\,\mathrm{g\,kg^{-1}}$	$-0.004\,\mathrm{g\,kg^{-1}}$
$\mathrm{S_{bottom}}$	$+0.006\,\mathrm{g\,kg^{-1}}$	$+0.003\,\mathrm{g\,kg^{-1}}$
HC	$+2.93 \times 10^{6}\,\mathrm{J\,m^{-2}}$	$-1.13 \times 10^{6}\,\mathrm{J\,m^{-2}}$
FW	$-0.548\,\mathrm{cm}$	$-0.091\,\mathrm{cm}$
$\mathrm{BC_{T+S}}$	$-0.20\,\mathrm{kg\,m^{-2}}$	$-0.12\,\mathrm{kg\,m^{-2}}$
$\mathrm{BC_{T}}$	$-0.34\,\mathrm{kg\,m^{-2}}$	$-0.24\,\mathrm{kg\,m^{-2}}$
$\mathrm{BC_{S}}$	$+0.14\,\mathrm{kg\,m^{-2}}$	$+0.12\,\mathrm{kg\,m^{-2}}$
IS	$-0.0029\,\mathrm{kg\,m^{-3}}$	$-0.0006\,\mathrm{kg\,m^{-3}}$
ERA5		
SST	$+0.033\,°\mathrm{C}$	$+0.013\,°\mathrm{C}$
P-E	$+0.014\,\mathrm{mm\,d^{-1}}$	$+0.038\,\mathrm{mm\,d^{-1}}$
BF	$+4.20 \times 10^{-10}\,\mathrm{W\,kg^{-1}}$	$+3.82 \times 10^{-10}\,\mathrm{W\,kg^{-1}}$
u^{*}	$+6.0 \times 10^{-6}\,\mathrm{m\,s^{-1}}$	$+2.0 \times 10^{-6}\,\mathrm{m\,s^{-1}}$
$\mathrm{Q_{net}}$	$+0.74\,\mathrm{W\,m^{-2}}$	$+0.67\,\mathrm{W\,m^{-2}}$
$\mathrm{Q_{shortwave}}$	$+0.045\,\mathrm{W\,m^{-2}}$	$+0.022\,\mathrm{W\,m^{-2}}$

Table 1: Linear trends of the main quantities. More estimates with detailed statistics are available in Supplementary Materials.

Year	$\overline{\text{MLD}}$ (m)	Start (week)	End (week)	τ (week)
2001	23.7	6	44	39
2002	26.9	15	42	28
2003	26.6	17	42	26
2004	19.8	13	47	35
2005	23.9	11	46	36
2006	28.9	12	44	33
2007	32.3	13	41	29
2008	30.8	12	42	31
2009	26.4	14	42	29
2010	25.4	9	41	33
2011	20.8	6	47	42
2012	25.4	12	47	36
2013	19.1	10	47	38
2014	20.0	8	45	38
2015	17.8	11	45	35
2016	22.5	10	45	36
2017	23.7	7	44	38
2018	26.0	14	44	31
2019	15.8	7	43	37

Table 2: Inter-annual averages of $\text{MLD}_{\sigma}^{0.03}$. Start and end refer to the weeks of the year when MLD $< 22m$ and $> 22m$; τ is the difference (+1).

	[2001-2009] All	Spring	Autumn	Winter	**[2010-2019]** All	Spring	Autumn	Winter
Data (N)	468	117	108	126	520	130	120	140
Training (N)	374	93	86	100	416	104	96	112
Validation (N)	94	24	22	26	104	26	24	28
$\overline{\text{MLD}}_{\text{valid}}(m)$	27.0	18.5	22.2	55.4	23.3	16.2	18.0	49.2
$\overline{\text{MLD}}_{\text{atlas}}(m)$	23.3	16.8	22.8	51.2	25.9	17.2	20.0	49.4
$\overline{\text{MLD}}_{\text{predi}}(m)$	26.8	15.5	22.6	58.4	24.0	16.2	17.2	39.6
$\overline{\lvert\text{MLD}_{\text{atlas}} - \text{MLD}_{\text{valid}}\rvert}(m)$	7.91	6.80	6.40	16.4	9.55	5.99	6.11	19.0
$\overline{\lvert\text{MLD}_{\text{predi}} - \text{MLD}_{\text{valid}}\rvert}(m)$	5.93	5.50	5.00	13.8	8.04	5.44	4.35	17.8
Accuracy (%) $= 100 - \overline{100 \times \lvert\text{predi} - \text{valid}\rvert/\text{valid}}$	73.8	78.1	73.9	57.2	59.3	69.9	78.8	52.7
Linear regression **$\text{MLD}_{\text{predi}}$ vs. $\text{MLD}_{\text{valid}}$**								
R^2	0.79	0.89	0.63	0.09	0.56	0.33	0.70	0.32
p-value	0.0	0.0	0.00001	0.12051	0.0	0.00186	0.0	0.00174
Corr. coef.	0.89	0.94	0.80	0.31	0.75	0.58	0.83	0.56

Table 3: Performance of the random forest regression. $\text{MLD}_{\text{valid}}$ refers to the fraction of data kept apart for the validation (not used during the training), $\text{MLD}_{\text{predi}}$ refers to the prediction, and $\text{MLD}_{\text{atlas}}$ refers to the averaged values established from the climatology, that would have been used as alternative estimates to observations or predictions.

7 Figures captions

Figure 1: Bathymetry and topography of the Gulf of Naples in Campania, Italy (data from GEBCO [2020]), along the Tyrrhenian Sea in the Mediterranean basin. In pink dots, the 75m-deep LTER-MC coastal sampling site ($14.25°E, 40.80°N$), and an offshore location to make a comparison to the coastal time series. Blue-green diamonds: the Volturno and Sarno's river mouths. Thin lines indicate the 50, 200, 300 and 400 m deep isobaths, and thick ones indicate 100, 500, 1000 and 2000 m deep.

Figure 2: Cilmatology of the temperature (left) and salinity (right), at the surface (top) and in the water-column (bottom), during the period 2001-2019. Top : seasonal cycles of surface temperature and salinity of the inshore observations at the LTER-MC point (gray points and plain lines), and the offshore data from the Med Sea reanalysis in the Tyrrhenian Sea (dashed lines). Bottom : monthly-averaged of vertical profiles of temperature and salinity, calculated from all the CTD profiles available (2001-2019). Black contours indicate the potential density σ_0 ($\mathrm{kg\,m^{-3}}$) ; plain white the $\mathrm{MLD}^{0.03}_{\sigma_0}$; dashed-white the $\mathrm{MLD}^{0.4}_{\theta_0}$.

Figure 3: Seasonal cycles of (a) heat content index ($\mathrm{J\,m^{-2}}$), (b) freshwater content index (cm), (c) intensity of stratification ($\mathrm{kg\,m^{-3}}$), (d) buoyancy content ($\mathrm{kg\,m^{-2}}$, decomposed by T in red, and S in blue), (e) heat content from fluxes (ERA5) integrated in time (vs. HC index in situ), (f) precipitation P and evaporation E rates ($\mathrm{mm\,d^{-1}}$, from ERA5)

.

Figure 4: From ERA5 parameters, (a) seasonal cycles of surface fluxes (total and shortwave, $\mathrm{J\,m^{-2}}$), (b) buoyancy fluxes ($\mathrm{W\,kg^{-1}}$), (c) significant sea wave height (m), (d) wind stress ($\mathrm{m\,s^{-1}}$), (e) wind velocities components ($\mathrm{m\,s^{-1}}$), and (f) wind direction (angular°)

Figure 5: Times series of the vertical profiles of the (a,c) temperature and (b,d) salinity anomalies, calculated as the difference to their associated seasonal cycles. Profiles have been averaged by months and main layers (centered on 2, 5, 10, 20, 30, 40, 50, 60 and 70 m) from the MC465 to MC1353 (January 2001 to December 2019).

Figure 6: Mean values of the (a) heat and (b) freshwater content anomalies, calculated by averaging over the season periods of the years.

Figure 7: Inter-annual cycles of quantities related to temperature (on the left), and to salinity (on the right). Straight lines refer to the linear trends (during 2001-2019, and 2005-2019, see Tab. 1). (a) Surface and bottom temperature (°C) (note the offset of 4 °C for the bottom temperature in dashed line, and in pink the SST from ERA5), (b) surface and bottom salinity ($\mathrm{g\,kg^{-1}}$), (c) heat content index ($\mathrm{J\,m^{-2}}$), (d) freshwater content index (cm), (e and f) buoyancy content ($\mathrm{kg\,m^{-2}}$, decomposed by T in red, and S in blue), (g) surface fluxes ($\mathrm{W\,m^{-1}}$, from ERA5), (h) rates of precipitation P and evaporation E ($\mathrm{mm\,d^{-1}}$, from ERA5).

Figure 8: (Top) Mean inter-annual values of the MLD (black line), and number of stratified weeks when $\mathrm{MLD}_{\sigma_0}^{0.03} < 22m$ (grey line). (Bottom). Mean inter-annual values of the MLD, decomposed by seasons (spring refers March-May ; summer to June-August ; autumn to September-November ; winter to December-February of the next year).

Figure 9: Inter-annual variability during the winter season.

Figure 10: MLD in function of the independent drivers, during the winter period in two decades (light blue : years [2001-2009]; dark blue : years [2010-2019]), representing the mechanical forcing (u^*), thermal convection (BF), the direction of wind, and the surface gradient between the GoN and the Tyrrhenian Sea (ΔS).

Figure 11: Importance of the relative contributors to the MLD's predictor, from the Random Forest Regressor, for each seasons between the decade I and II.

Figures for "Long-term variability of the coastal ocean stratification in the Gulf of Naples: Two decades of monitoring the marine ecosystem at the LTER-MC site, between land and open Mediterranean sea"

Florian Kokoszka[1], Baptiste Le Roux[2], Daniele Iudicone[1], Fabio Conversano[1], and Maurizio Ribera d'Alcalá[1]

[1]Stazione Zoologica Anton Dohrn, Naples, Italy
[2]Ecole Centrale de Nantes, Nantes, France

Corresponding author: Florian Kokoszka, florian.kokoszka@szn.it

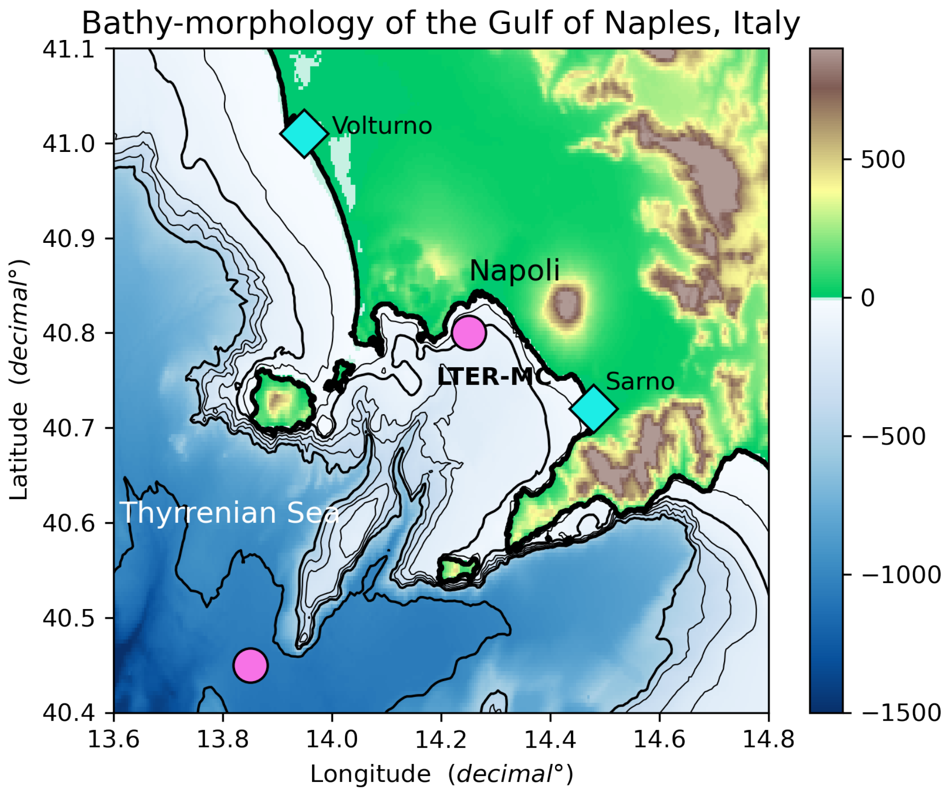

Figure 1: Bathymetry and topography of the Gulf of Naples in Campania, Italy (data from GEBCO [2020]), along the Tyrrhenian Sea in the Mediterranean basin. In pink dots, the 75m-deep LTER-MC coastal sampling site ($14.25°E, 40.80°N$), and an offshore location to make a comparison to the coastal time series. Blue-green diamonds: the Volturno and Sarno's river mouths. Thin lines indicate the 50, 200, 300 and 400 m deep isobaths, and thick ones indicate 100, 500, 1000 and 2000 m deep.

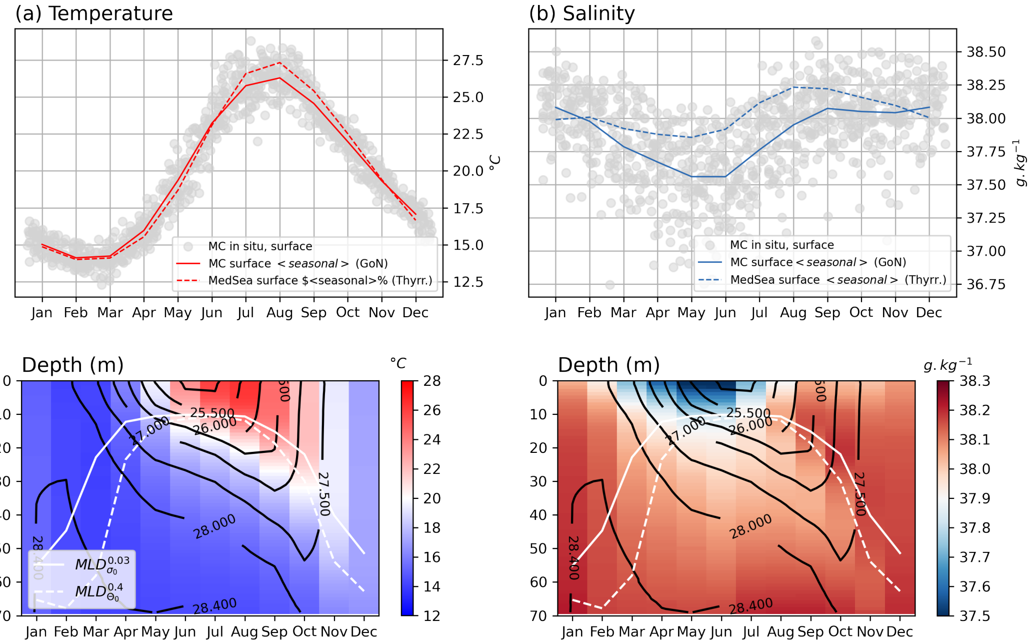

Figure 2: Cilmatology of the temperature (left) and salinity (right), at the surface (top) and in the water-column (bottom), during the period 2001-2019. Top : seasonal cycles of surface temperature and salinity of the inshore observations at the LTER-MC point (gray points and plain lines), and the offshore data from the Med Sea reanalysis in the Tyrrhenian Sea (dashed lines). Bottom : monthly-averaged of vertical profiles of temperature and salinity, calculated from all the CTD profiles available (2001-2019). Black contours indicate the potential density σ_0 ($\mathrm{kg\,m^{-3}}$) ; plain white the $\mathrm{MLD}^{0.03}_{\sigma_0}$; dashed-white the $\mathrm{MLD}^{0.4}_{\theta_0}$.

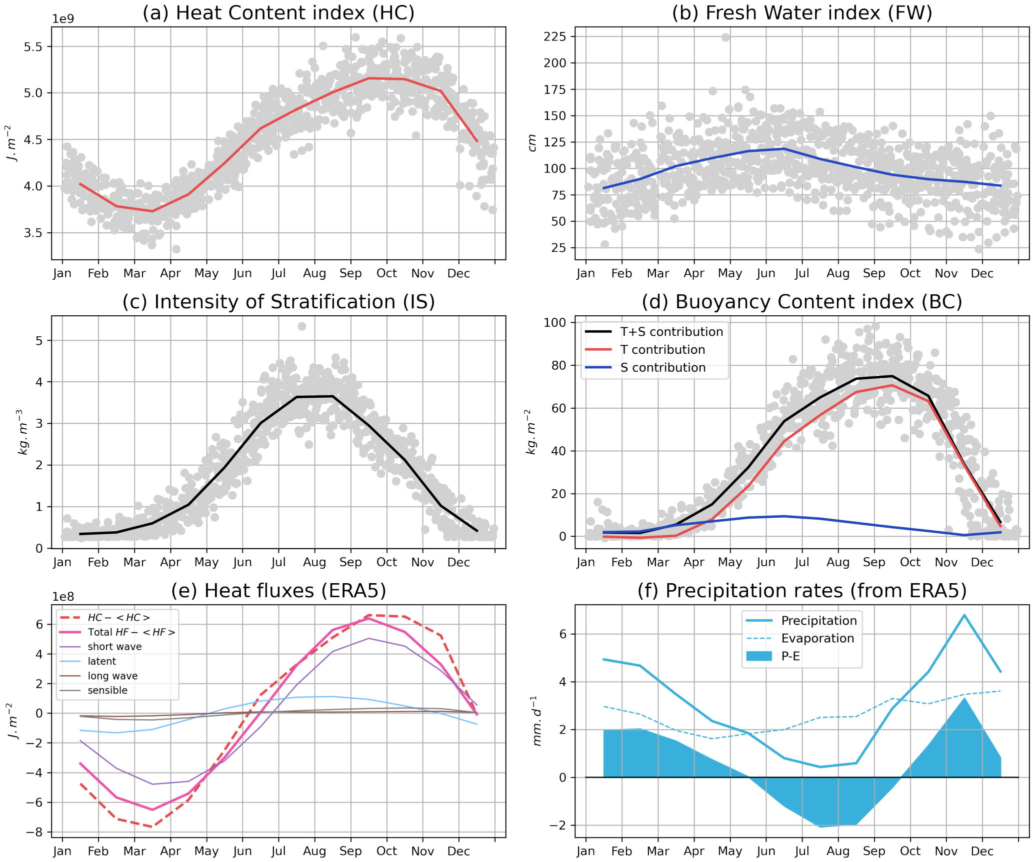

Figure 3: Seasonal cycles of (a) heat content index ($\mathrm{J\,m^{-2}}$), (b) freshwater content index (cm), (c) intensity of stratification ($\mathrm{kg\,m^{-3}}$), (d) buoyancy content ($\mathrm{kg\,m^{-2}}$, decomposed by T in red, and S in blue), (e) heat content from fluxes (ERA5) integrated in time (vs. HC index in situ), (f) precipitation P and evaporation E rates ($\mathrm{mm\,d^{-1}}$, from ERA5)

.

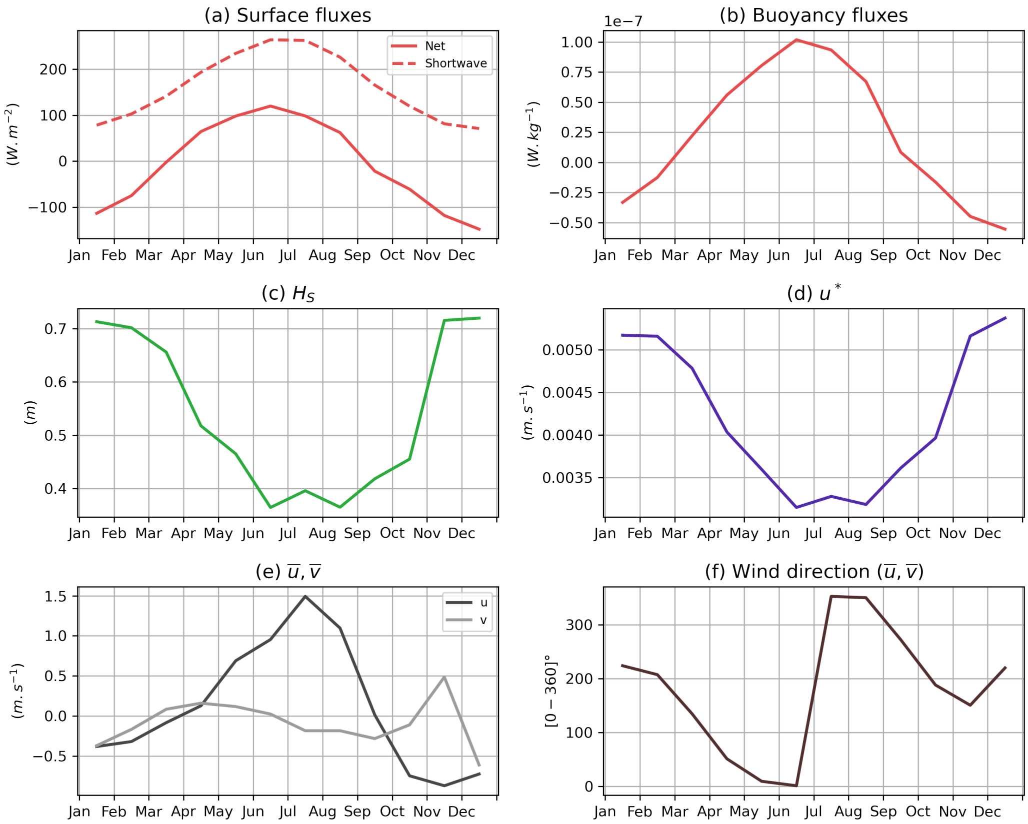

Figure 4: From ERA5 parameters, (a) seasonal cycles of surface fluxes (total and shortwave, $\mathrm{J\,m^{-2}}$), (b) buoyancy fluxes ($\mathrm{W\,kg^{-1}}$), (c) significant sea wave height (m), (d) wind stress ($\mathrm{m\,s^{-1}}$), (e) wind velocities components ($\mathrm{m\,s^{-1}}$), and (f) wind direction (angular°)

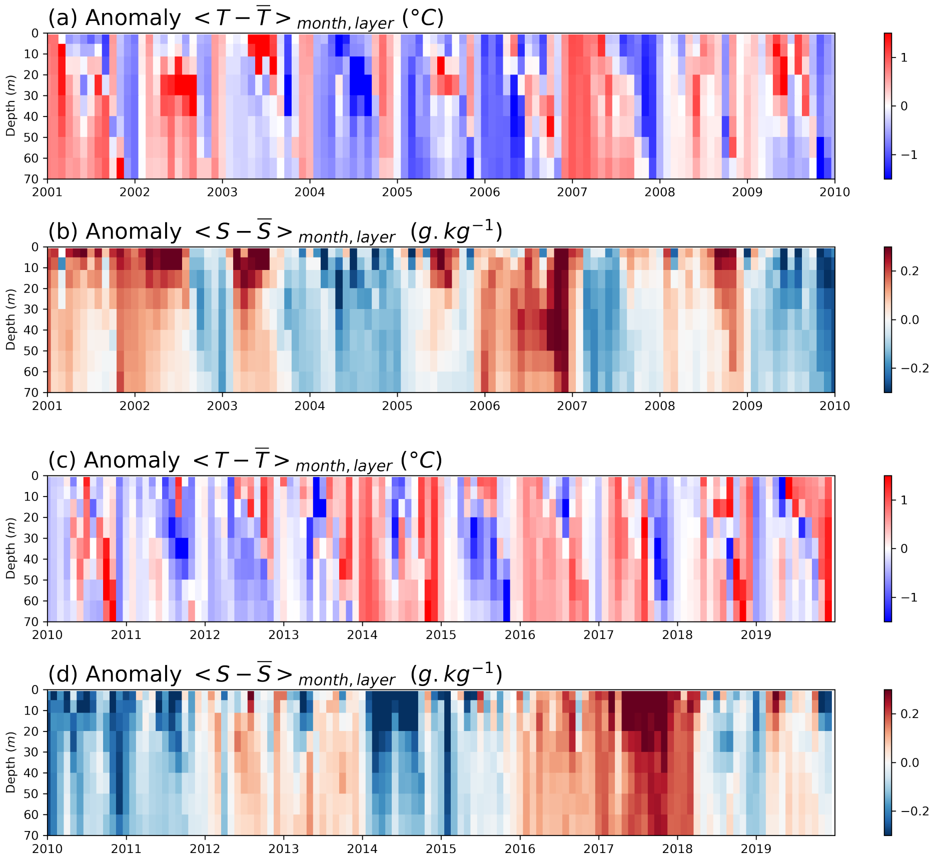

Figure 5: Times series of the vertical profiles of the (a,c) temperature and (b,d) salinity anomalies, calculated as the difference to their associated seasonal cycles. Profiles have been averaged by months and main layers (centered on 2, 5, 10, 20, 30, 40, 50, 60 and 70 m) from the MC465 to MC1353 (January 2001 to December 2019).

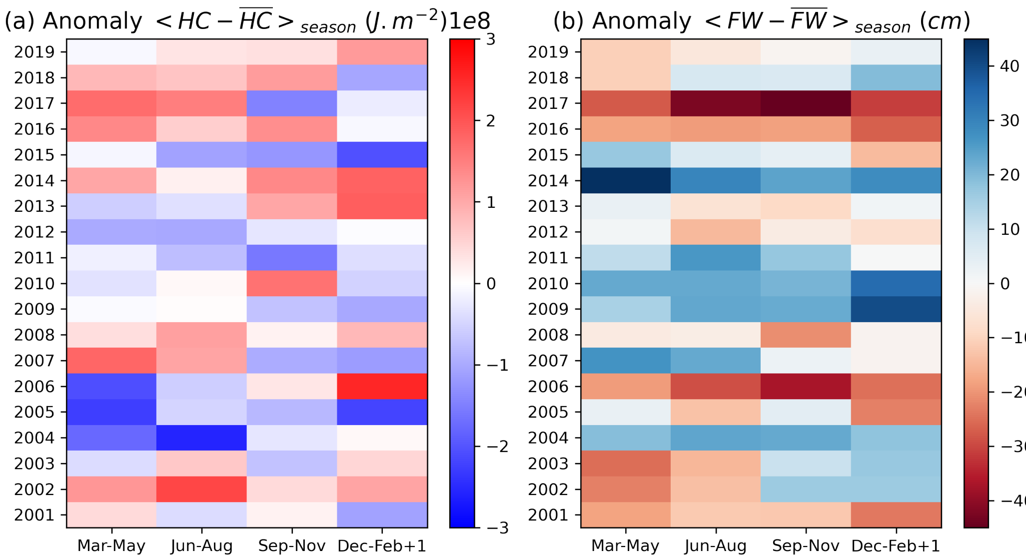

Figure 6: Mean values of the (a) heat and (b) freshwater content anomalies, calculated by averaging over the season periods of the years.

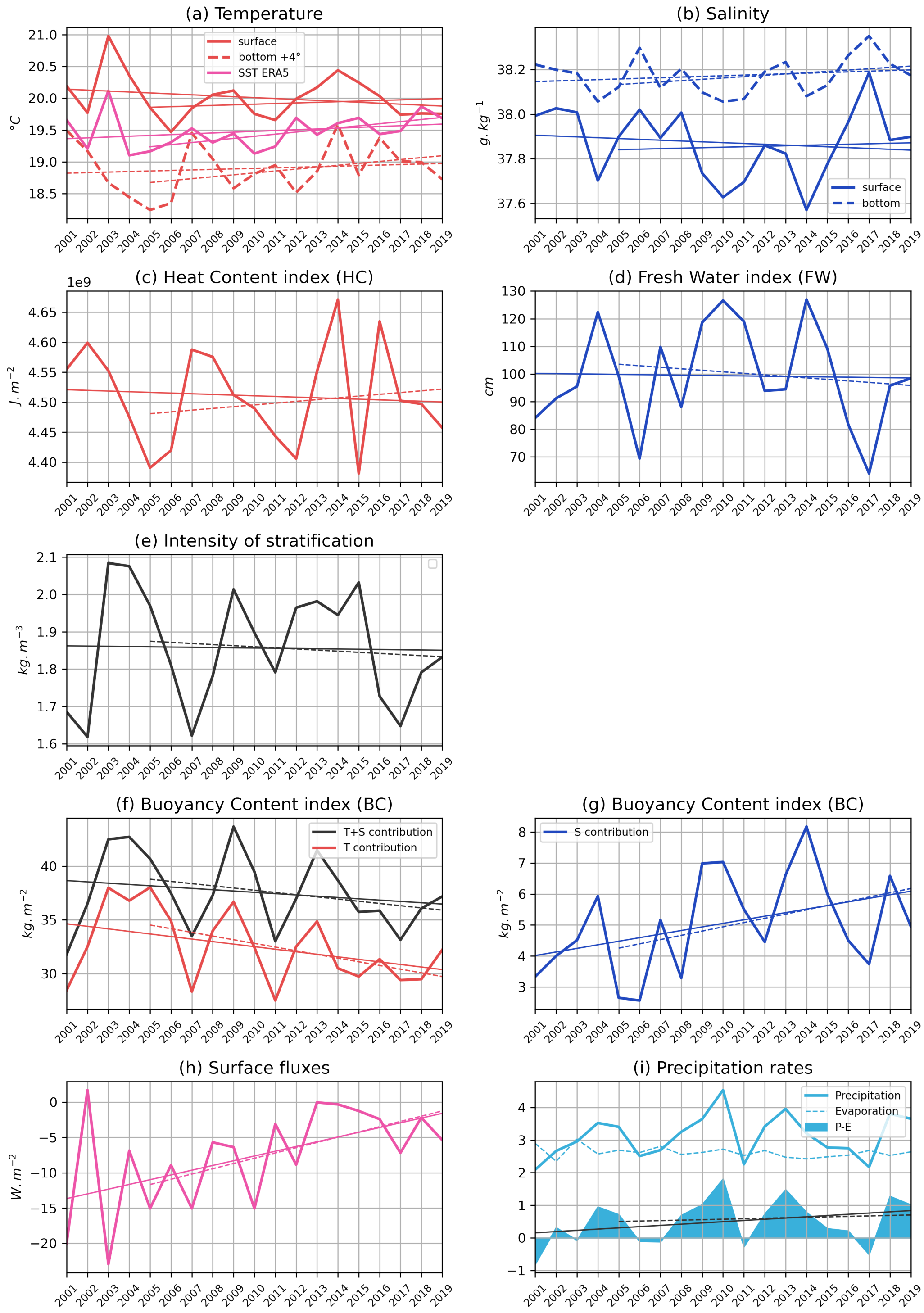

Figure 7: Inter-annual cycles of quantities related to temperature (on the left), and to salinity (on the right). Straight lines refer to the linear trends (during 2001-2019, and 2005-2019, see Tab. 1). (a) Surface and bottom temperature (°C) (note the offset of 4 °C for the bottom temperature in dashed line, and in pink the SST from ERA5), (b) surface and bottom salinity (g kg^{-1}), (c) heat content index (J m^{-2}), (d) freshwater content index (cm), (e and f) buoyancy content (kg m^{-2}, decomposed by T in red, and S in blue), (g) surface fluxes (W m^{-1}, from ERA5), (h) rates of precipitation P and evaporation E (mm d^{-1}, from ERA5).

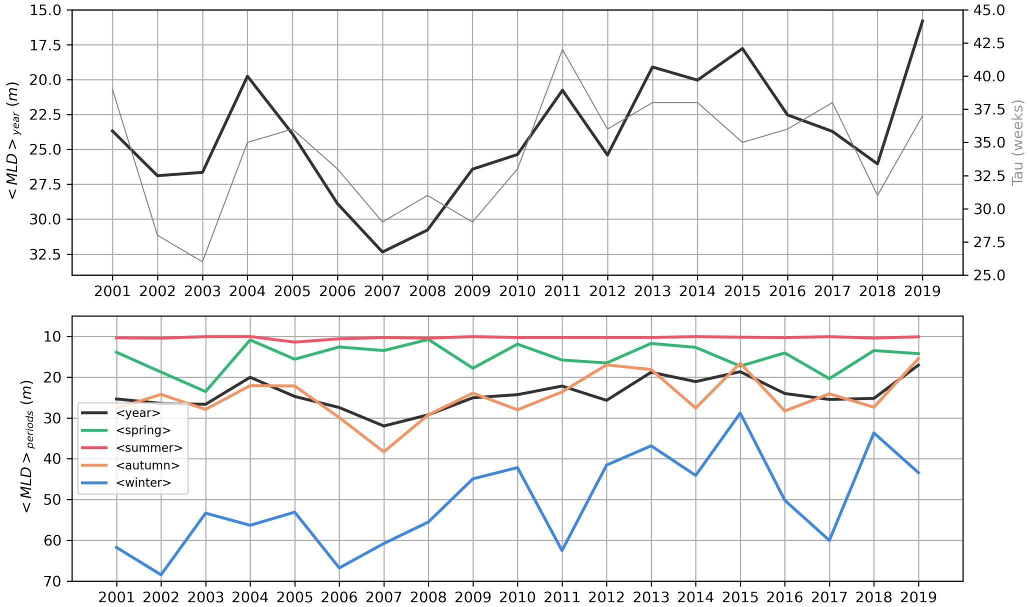

Figure 8: (Top) Mean inter-annual values of the MLD (black line), and number of stratified weeks when $\mathrm{MLD}^{0.03}_{\sigma_0} < 22m$ (grey line). (Bottom). Mean inter-annual values of the MLD, decomposed by seasons (spring refers March-May ; summer to June-August ; autumn to September-November ; winter to December-February of the next year).

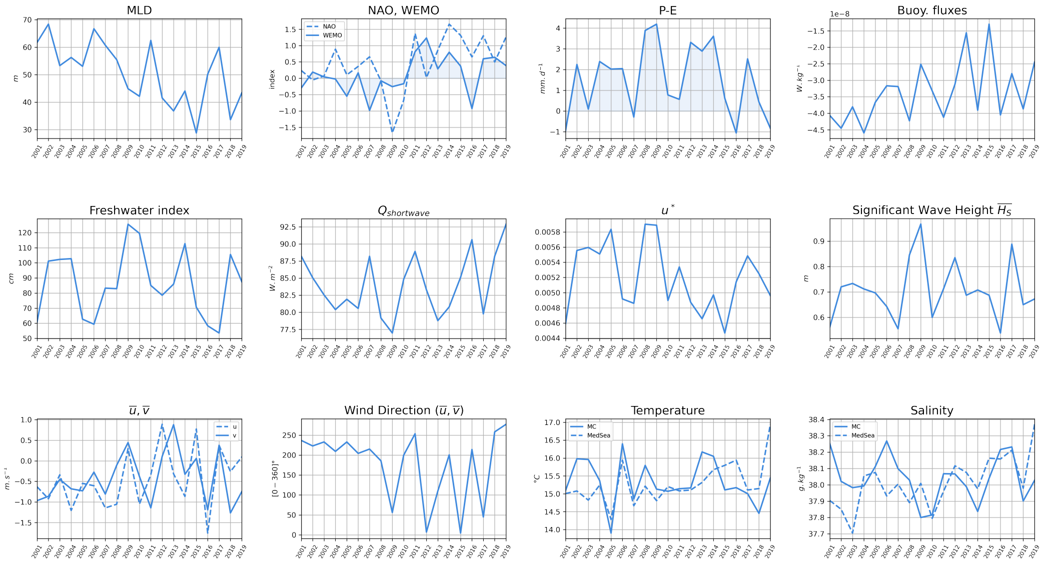

Figure 9: Inter-annual variability during the winter season.

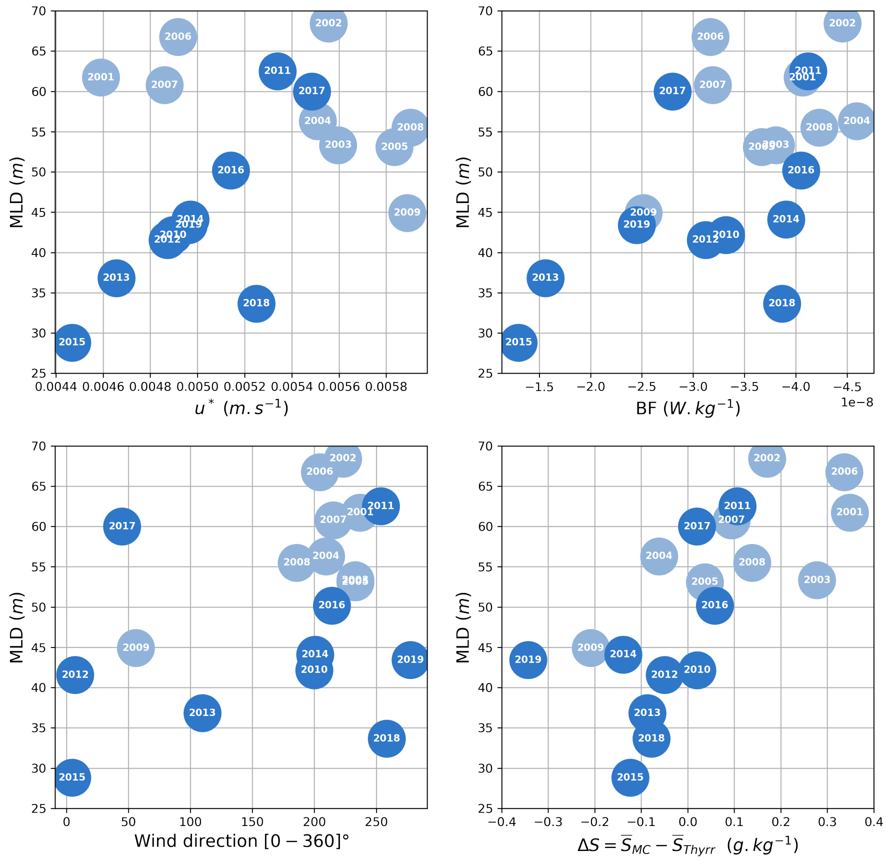

Figure 10: MLD in function of the independent drivers, during the winter period in two decades (light blue : years [2001-2009]; dark blue : years [2010-2019]), representing the mechanical forcing (u^*), thermal convection (BF), the direction of wind, and the surface gradient between the GoN and the Tyrrhenian Sea (ΔS).

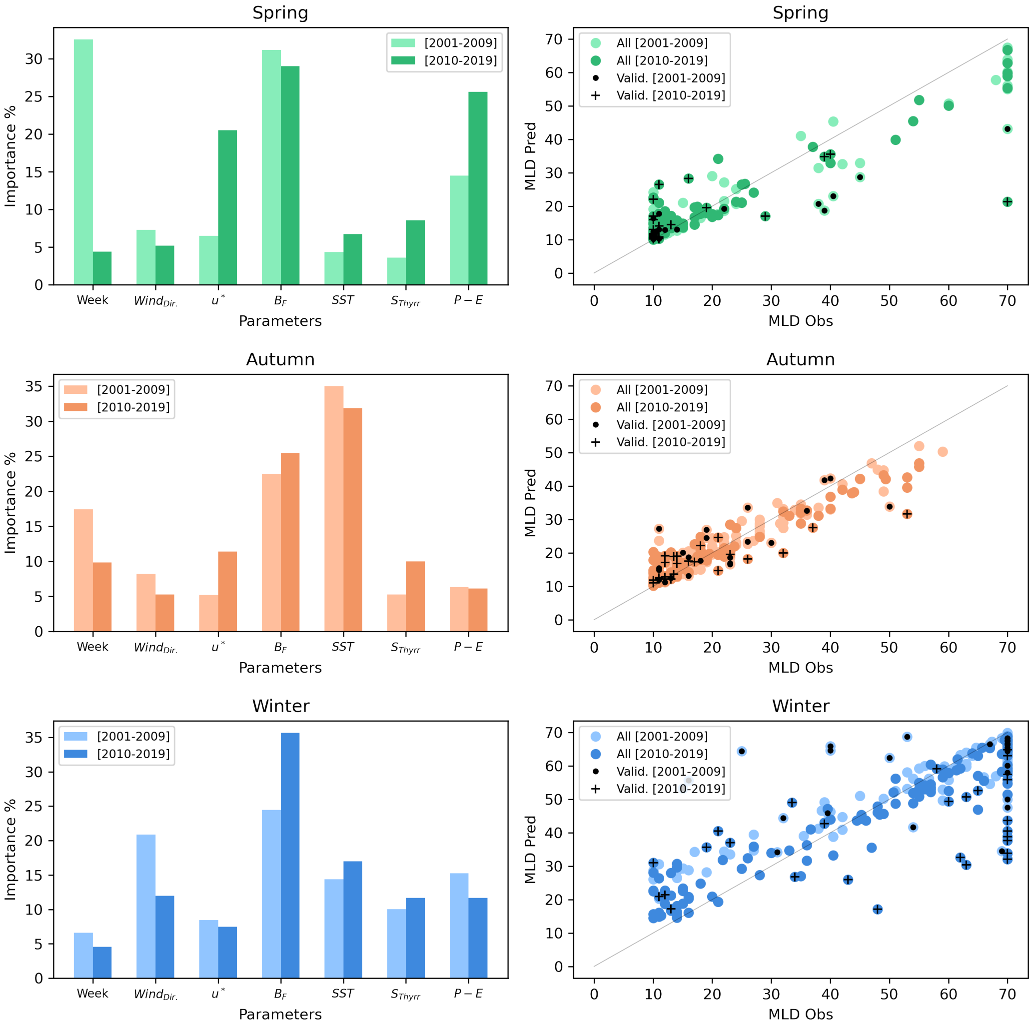

Figure 11: Importance of the relative contributors to the MLD's predictor, from the Random Forest Regressor, for each seasons between the decade I and II.

Supporting Information for "Long-term variability of the coastal ocean stratification in the Gulf of Naples: Two decades of monitoring the marine ecosystem at the LTER-MC site, between land and open Mediterranean sea"

Florian Kokoszka[1], Baptiste Le Roux[2], Daniele Iudicone[1], Fabio Conversano[1], and Maurizio Ribera d'Alcalá[1]

[1]Stazione Zoologica Anton Dohrn, Naples, Italy

[2]Ecole Centrale de Nantes, Nantes, France

We provide in Fig. S1 the calendar of the CTD casts (referenced as MC). We provide in Fig. S2 the time series of the variables used in the study. These variables are decomposed into 5 time series (inter-annual, and the four inter-annual of seasons). For each one, we calculate linear fits and export statistical values (slope, slope 95% confidence interval, R^2, p-value, STD error and intercept) and values of the time series (from 2001 to 2019). We proceed over four periods : 2001-2019, 2005-2019 (to exclude the heatwave of 2003), then 2001-2009 (decade I), and 2010-2019 (decade II). Raw results for each period are provided in four separated `.csv` data-frames files: `df_MC_TRENDS_2001_2019.csv`, `df_MC_TRENDS_2001_2009.csv`, `df_MC_TRENDS_2010_2019.csv` and `df_MC_TRENDS_2005_2019.csv`.

Corresponding author: F. Kokoszka, Department of Research Infrastructures for Marine Biological Resources (RIMAR), Stazione Zoologica A. Dohrn, villa Comunale, 80121, Naples, Italy (florian.kokoszka@szn.it)

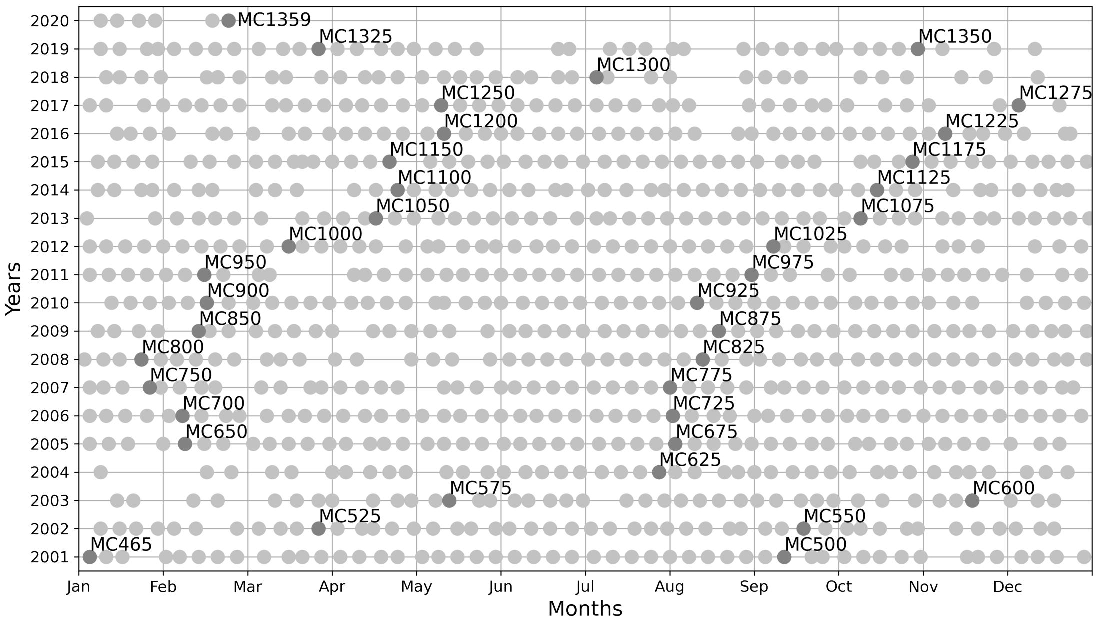

Figure S1. Calendar of the CTD profiles : 894 CTD profiles from the 4th January 2001 (cast MC465) to the 24th February 2020 (cast MC1359).

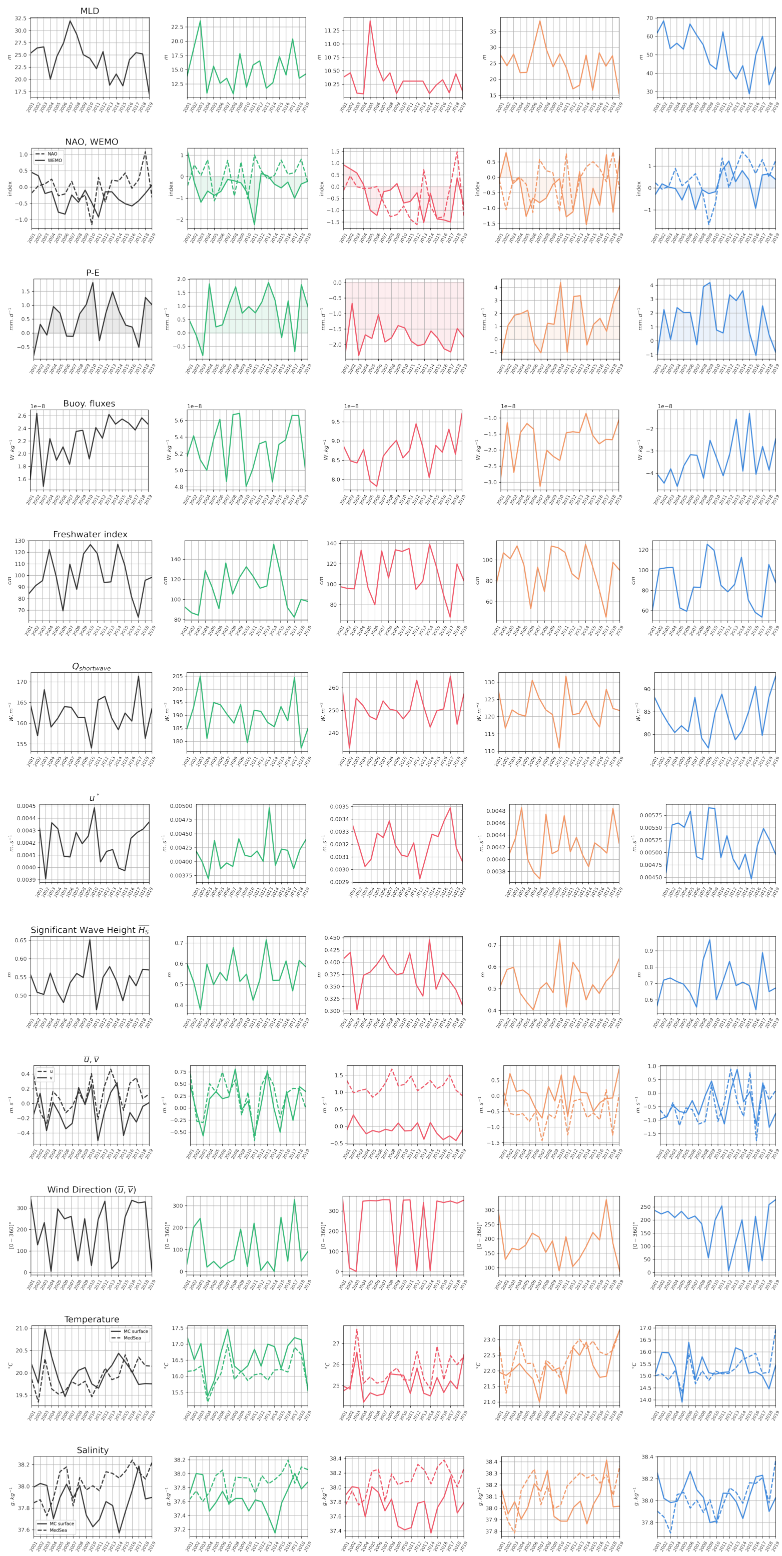

Figure S2. Time series of the variables used in the study : full year inter-annual in black, and inter-annual of seasons in color (spring, summer, autumn, winter, in green, red, orange and blue).